

STUDY OF THERMAL RADIATION AND CHEMICAL REACTION EFFECTS ON MHD FLOW IN POROUS MEDIUM

Influence of thermal radiation effect plays significant role in controlling heat transfer process in polymer processing industry. In several new manufacturing areas, progresses occur at high temperatures so understanding of radiation heat transfer besides the convective heat transfer play essential role and cannot be ignored. The Rosseland approximation is used to describe the radiative heat flux in the energy equation. The chemical reaction can be classified as either a heterogeneous or a homogeneous process. This depends on whether it occurs at an interface or as a single-phase volume reaction. A few representative fields of interest where combined heat and mass transfer with a chemical reaction and thermal radiation plays an important role are design of chemical processing equipment, cooling towers, etc.

This chapter contains two sections, in first section, effects of thermal radiation, chemical reaction and magnetic field on Casson fluid past an oscillating plate embedded in porous medium is considered with ramped wall temperature. Second section of this chapter deals with mathematical analysis of MHD flow of radiative and chemically reactive Casson fluid past over an exponentially accelerated plated embedded in porous medium with ramped boundary conditions.

4.1 SECTION I: RADIATION AND CHEMICAL REACTION EFFECTS ON MHD CASSON FLUID FLOW PAST AN OSCILLATING VERTICAL PLATE EMBEDDED IN POROUS MEDIUM

This section deals with mathematical modelling of thermal radiation and chemical reaction effects on Casson fluid flow with magnetic field past an oscillating vertical plate embedded in porous medium. Suppose that the bounding plate of this problem are ramped as well as isothermal temperature. For both thermal plates, governing dimensionless equations are solved analytically using Laplace transform method. To analyze effects of thermal radiation and chemical reaction on momentum, numerical values from analytical results are obtained and presented in graphs. Expression for shear stress, temperature gradient and concentration gradient are derived and presented in tabular form.

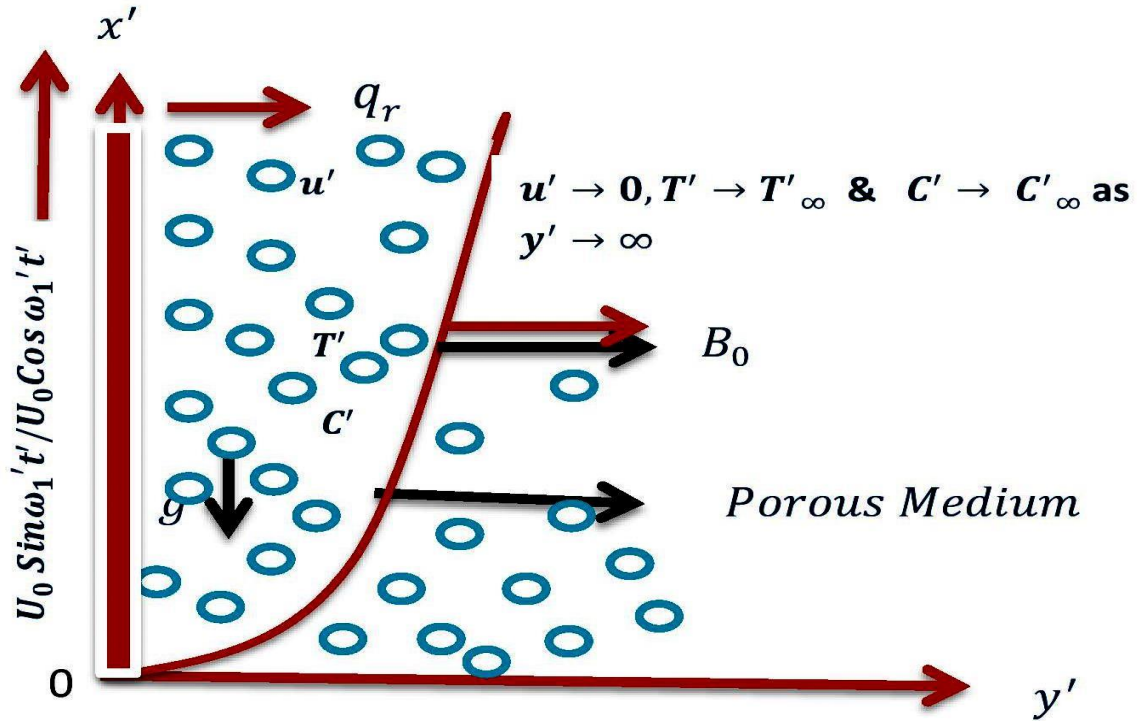
4.1.1 Introduction of the Problem

The study of MHD flow of non-Newtonian fluid in a porous medium has attracted many researchers due to its applications in optimization of solidification processes of metals, alloys, the geothermal sources investigation and nuclear fuel debris treatment. Recently, Nadeem et al. [88] studied MHD flow of a Casson fluid over a linearly shrinking sheet, whereas Nadeem et al. [50] discussed three-dimensional boundary layer flow of Casson nanofluid with magnetic field past a linearly stretching sheet. Thermal radiation parameter effects may play a significant role in controlling heat transfer in polymer processing industry. Makanda et al. [94] studied effects of radiation on MHD flow of Casson fluid from a horizontal circular cylinder in non-Darcy porous medium. Sheikholeslami [99-100] considered thermal radiation effects on MHD nanofluid flow. Rashidi et al. [103] and Ahmed et al. [104] deliberated MHD flow in the presence of the radiation in porous medium. Applications of heat and mass transfer flow with chemical reaction can be found in catalytic chemical reactors, food processing, polymer production, manufacture of ceramics and glassware etc. Animasaun [107] and Makanda et al. [108] studied chemical reaction on unsteady flow of Casson fluid. Research work on combined effects of thermal radiation and chemical reaction on MHD flow which is done by Reddy [111] and Nayak et al. [112]. Soundalgekar [159], first obtained analytical solutions of free convective flow past an oscillating vertical plate and the same problem with mass transfer effect was considered by Soundalgekar and Akolkar [160]. The oscillatory motion is usual in industries when the oscillating surfaces are embedded in a porous medium. Recently, Khalid et al. [89] deliberated effects of magnetic field on Casson fluid flow past an oscillating plate in porous medium, whereas Kataria and Mittal [96-97] considered MHD nano fluid flow past an oscillating vertical plate.

4.1.2 Novelty of the Problem

In present investigation, combined effects of thermal radiation and chemical on unsteady free convective MHD flow of Casson fluid past over an oscillating vertical plate embedded in porous medium with ramped and isothermal wall temperature is considered. Analytic expressions for velocity, temperature and concentration profiles are obtained with the help of Laplace transform technique. As it is discussed analytical results, unlike numerical work of different authors, convergence of solution is not an issue.

4.1.3. Mathematical formulation of the problem



$$T' = \begin{cases} T'_\infty + (T'_w - T'_\infty) t'/t_0 & \text{if } 0 < t' < t_0 \\ T'_w & \text{if } t' \geq t_0 \end{cases} \quad \& C' = C'_\infty + (C'_w - C'_\infty) t'/t_0; t' \geq 0 \text{ and } y' = 0$$

Figure 4.1.1: Physical sketch of the problem

In Figure 4.1.1, the flow is being confined to $y' > 0$, where y' is the coordinate measured in the normal direction to the plate and x' – axis is taken along the wall in the upward direction. Initially, at time $t' = 0$, both the fluid and the plate are at uniform temperature T'_∞ and the concentration near the plate is assumed to be C'_∞ at all the points respectively. At time $t' > 0$, the plate is given an oscillatory motion in the vertical direction against gravitational field with velocity $U_0 \sin(\omega_1 t')$ or $U_0 \cos(\omega_1 t')$. At time $t' > 0$, the temperature of the plate is raised or lowered to $T'_\infty + (T'_w + T'_\infty) t'/t_0$ when $t' < t_0$ and T'_w when $t' > t_0$ respectively which is there after maintained constant T'_w and surface concentration near the plate is raised linearly to $C'_\infty + (C'_w + C'_\infty) t'/t_0$ which is there after maintained constant C'_w . A uniformly distributed transverse

magnetic field of strength B_0 is applied in the y' – axis direction. Under these condition, the following partial differential equation with initial and boundary condition are given below.

$$\rho \frac{\partial u'}{\partial t'} = \mu\beta \left(1 + \frac{1}{\nu}\right) \frac{\partial^2 u'}{\partial y'^2} - \sigma B_0^2 u' - \frac{\mu\phi}{k'} u' + \rho g\beta'_T (T' - T'_\infty) + \rho g\beta'_C (C' - C'_\infty) \quad (4.1.1)$$

$$\frac{\partial T'}{\partial t'} = \frac{k_4}{\rho c_p} \frac{\partial^2 T'}{\partial y'^2} - \frac{1}{\rho c_p} \frac{\partial q_{r'}}{\partial y'} \quad (4.1.2)$$

$$\frac{\partial C'}{\partial t'} = D_M \frac{\partial^2 C'}{\partial y'^2} - k'_2 (C' - C'_\infty) \quad (4.1.3)$$

$$u' = 0, \quad T' = T'_\infty, \quad C' = C'_\infty; \text{ as } y' \geq 0 \text{ and } t' \leq 0$$

$$u' = U_0 \sin(\omega_1 t') \text{ or } U_0 \cos(\omega_1 t'), T' = \begin{cases} T'_\infty + (T'_w - T'_\infty) t'/t_0 & \text{if } 0 < t' < t_0 \\ T'_w & \text{if } t' \geq t_0 \end{cases},$$

$$C' = C'_\infty + (C'_w - C'_\infty) t'/t_0; t' \geq 0 \text{ and } y' = 0$$

$$u' \rightarrow 0, T' \rightarrow T'_\infty, \quad C' \rightarrow C'_\infty; \text{ as } y' \rightarrow \infty \text{ and } t' \geq 0 \quad (4.1.4)$$

The local radiant for the case of an optically thin gray gas is expressed by Rosseland approximation [91]

$$\frac{\partial q_{r'}}{\partial y'} = -4a^* \sigma^* (T'^4_\infty - T'^4) \quad (4.1.5)$$

where σ^* and a^* are Stefan Boltzmann constant and absorption coefficient respectively.

Using the Taylor's series, expand T'^4 about T'_∞ and neglecting higher order terms,

$$T'^4 \cong 4T'^3_\infty T' - 3T'^4_\infty \quad (4.1.6)$$

Substituting values from (4.1.6) and (4.1.5) in (4.1.2)

$$\frac{\partial T'}{\partial t'} = \frac{k_4}{\rho c_p} \frac{\partial^2 T'}{\partial y'^2} + \frac{1}{\rho c_p} 16a^* \sigma^* T'^3_\infty (T' - T'_\infty) \quad (4.1.7)$$

Introducing the following dimensionless quantities:

$$y = \frac{U}{\nu t_0} y', t = \frac{U^2 t}{\nu t_0}, u = \frac{\sqrt{t_0}}{U} u, \theta = \frac{T - T_\infty}{T_w - T_\infty}, C = \frac{C - C_\infty}{C_w - C_\infty}, W = \frac{w \nu}{U^2}, Pr = \frac{\rho c_p}{k_4}, \tau = \frac{\tau}{\rho u^2}$$

$$M^2 = \frac{\sigma B_0^2}{\rho U_0^2} t_0, \frac{1}{k} = \frac{\nu \phi^2}{k' U_0^2}, Gr = \frac{\nu g \beta (T_w - T_\infty)}{U_0^3}, \gamma = \frac{\mu_B \sqrt{2\pi c}}{P_y}, Sc = \frac{\nu}{D_M}, Gm = \frac{g \beta_c \nu (C_w - C_\infty)}{U_0^3}$$

$$Nr = -\frac{16 a^* \sigma^* v^2 T'_{\infty}{}^3}{k_4 U_0^2}, Kr = \frac{\nu k_2'}{U_0^2},$$

In the equations (4.1.1) to (4.1.4) dropping out the " ' " notation (for simplicity),

$$\frac{\partial u}{\partial t} = \left(1 + \frac{1}{\gamma}\right) \frac{\partial^2 u}{\partial y^2} - \left(M^2 + \frac{1}{k}\right) u + G_r \theta + G_m C \quad (4.1.8)$$

$$\frac{\partial \theta}{\partial t} = \frac{1}{Pr} \frac{\partial^2 \theta}{\partial y^2} - \frac{Nr}{Pr} \theta \quad (4.1.9)$$

$$\frac{\partial C}{\partial t} = \frac{1}{s_c} \frac{\partial^2 C}{\partial y^2} - Kr C \quad (4.1.10)$$

with initial and boundary condition

$$u = \theta = C = 0, \quad y > 0, t < 0$$

$$u = \sin(\omega_1 t) \text{ or } H(t) \cos(\omega_1 t),$$

$$\theta = \begin{cases} t, & 0 < t \leq 1 \\ 1 & t > 1 \end{cases} = tH(t) - (t-1)H(t-1), \quad C = t \text{ at } y = 0, t \geq 0$$

$$u \rightarrow 0, \theta \rightarrow 0, C \rightarrow 0 \quad \text{at } y \rightarrow \infty \quad (4.1.11)$$

4.1.4. Solution of the Problem

Taking Laplace transform of equations (4.1.8) to (4.1.10) with initial and boundary conditions (4.1.11)

$$\bar{\theta}(y, s) = F_9(y, s)(1 - e^{-s}) \quad (4.1.12)$$

$$\bar{C} = F_{11}(y, s) \quad (4.1.13)$$

$$\begin{aligned} \bar{u}_{sin}(y, s) = & \frac{i}{2} F_1(y, s) - \frac{i}{2} F_2(y, s) + (1 - e^{-s}) G_1(y, s) + a_{10} F_4(y, s) + a_{11} F_5(y, s) + \\ & a_{12} F_6(y, s) - (1 - e^{-s}) G_2(y, s) - a_{10} F_{10}(y, s) - a_{12} F_{11}(y, s) - a_{12} F_{12}(y, s) \end{aligned} \quad (4.1.14)$$

$$\begin{aligned} \bar{u}_{cos}(y, s) = & \frac{1}{2} F_1(y, s) + \frac{1}{2} F_2(y, s) + (1 - e^{-s}) G_1(y, s) + a_{10} F_4(y, s) + a_{11} F_5(y, s) + \\ & a_{12} F_6(y, s) - (1 - e^{-s}) G_9(y, s) - a_{10} F_{12}(y, s) - a_{11} F_{11}(y, s) - a_{12} F_{12}(y, s) \end{aligned} \quad (4.1.15)$$

$$F_1(y, s) = \frac{e^{-y\sqrt{\frac{s+b}{a}}}}{s+i\omega_1} \quad (4.1.16)$$

$$F_2(y, s) = \frac{e^{-y\sqrt{\frac{s+b}{a}}}}{s-i\omega_1} \quad (4.1.17)$$

$$G_1(y, s) = a_7F_3(y, s) + a_8F_4(y, s) + a_9F_5(y, s) \quad (4.1.18)$$

$$F_3(y, s) = \frac{e^{-y\sqrt{\frac{s+b}{a}}}}{s+a_3} \quad (4.1.19)$$

$$F_4(y, s) = \frac{e^{-y\sqrt{\frac{s+b}{a}}}}{s} \quad (4.1.20)$$

$$F_5(y, s) = \frac{e^{-y\sqrt{\frac{s+b}{a}}}}{s^2} \quad (4.1.21)$$

$$F_6(y, s) = \frac{e^{-y\sqrt{\frac{s+b}{a}}}}{s+a_6} \quad (4.1.22)$$

$$G_2(y, s) = a_7F_7(y, s) + a_8F_8(y, s) + a_9F_9(y, s) \quad (4.1.23)$$

$$F_7(y, s) = \frac{e^{-y\sqrt{Nr+Prs}}}{s+a_3} \quad (4.1.24)$$

$$F_8(y, s) = \frac{e^{-y\sqrt{Nr+Prs}}}{s} \quad (4.1.25)$$

$$F_9(y, s) = \frac{e^{-y\sqrt{Nr+Prs}}}{s^2} \quad (4.1.26)$$

$$F_{10}(y, s) = \frac{1}{s} e^{-y\sqrt{s_c(Kr+s)}} \quad (4.1.27)$$

$$F_{11}(y, s) = \frac{1}{s^2} e^{-y\sqrt{s_c(Kr+s)}} \quad (4.1.28)$$

$$F_{12}(y, s) = \frac{1}{(s+a_6)} e^{-y\sqrt{s_c(Kr+s)}} \quad (4.1.29)$$

Taking inverse Laplace transform of equations (4.1.12) to (4.1.29),

4.1.4.1 Solutions for Plate with ramped wall temperature

$$\theta(y, t) = f_9(y, t) - f_9(y, t - 1)H(t - 1) \quad (4.1.30)$$

$$C(y, t) = f_{11}(y, t) \quad (4.1.31)$$

$$\begin{aligned}
 u_{sin}(y, t) = & \frac{i}{2}f_1(y, t) - \frac{i}{2}f_2(y, t) + g_1(y, t) - g_1(y, t - 1)H(t - 1) + a_{10}f_4(y, t) + \\
 & a_{11}f_5(y, t) + a_{12}f_6(y, t) - g_2(y, t) + g_2(y, t - 1)H(t - 1) - a_{10}f_{10}(y, t) - \\
 & a_{11}f_{11}(y, t) - a_{12}f_{12}(y, t)
 \end{aligned} \tag{4.1.32}$$

$$\begin{aligned}
 u_{cos}(y, t) = & \frac{1}{2}f_1(y, t) + \frac{1}{2}f_2(y, t) + g_1(y, t) - g_1(y, t - 1)H(t - 1) + a_{10}f_4(y, t) + \\
 & a_{11}f_5(y, t) + a_{12}f_6(y, t) - g_2(y, t) + g_2(y, t - 1)H(t - 1) - a_{10}f_{10}(y, t) - \\
 & a_{11}f_{11}(y, t) - a_{12}f_{12}(y, t)
 \end{aligned} \tag{4.1.33}$$

4.1.4.2 Solutions for Plate with isothermal temperature

In this case, the initial and boundary conditions are the same excluding Eq. (4.1.11) that becomes $\theta = 1$ at $y = 0, t \geq 0$. So, expression of velocity, temperature and concentration profiles are obtained for isothermal temperature which is given below.

$$\theta(y, t) = f_8(y, t) \tag{4.1.34}$$

$$C(y, t) = f_{11}(y, t) \tag{4.1.35}$$

$$\begin{aligned}
 u_{sin}(y, t) = & \frac{i}{2}f_1(y, t) - \frac{i}{2}f_2(y, t) + (a_9 + a_{10})f_4(y, t) - a_9f_3(y, t) + a_{11}f_5(y, t) + \\
 & a_{12}f_6(y, t) - a_9f_8(y, t) + a_9f_7(y, t) - a_{10}f_{10}(y, t) - a_{11}f_{11}(y, t) - a_{12}f_{12}(y, t)
 \end{aligned} \tag{4.1.36}$$

$$\begin{aligned}
 u_{cos}(y, t) = & \frac{1}{2}f_1(y, t) + \frac{1}{2}f_2(y, t) + (a_9 + a_{10})f_4(y, t) - a_9f_3(y, t) + a_{11}f_5(y, t) + \\
 & a_{12}f_6(y, t) - a_9f_8(y, t) + a_9f_7(y, t) - a_{10}f_{10}(y, t) - a_{11}f_{11}(y, t) - a_{12}f_{12}(y, t)
 \end{aligned} \tag{4.1.37}$$

Where

$$\begin{aligned}
 f_1(y, t) = & \frac{e^{-i\omega_1 t}}{2} \left[e^{-y\sqrt{\frac{1}{a}(b-i\omega_1)}} \operatorname{erfc} \left(\frac{y}{2\sqrt{at}} - \sqrt{(b-i\omega_1)t} \right) + e^{y\sqrt{\frac{1}{a}(b-i\omega_1)}} \operatorname{erfc} \left(\frac{y}{2\sqrt{at}} + \right. \right. \\
 & \left. \left. \sqrt{(b-i\omega_1)t} \right) \right]
 \end{aligned} \tag{4.1.38}$$

$$\begin{aligned}
 f_2(y, t) = & \frac{e^{i\omega_1 t}}{2} \left[e^{-y\sqrt{\frac{1}{a}(b+i\omega_1)}} \operatorname{erfc} \left(\frac{y}{2\sqrt{at}} - \sqrt{(b+i\omega_1)t} \right) + e^{y\sqrt{\frac{1}{a}(b+i\omega_1)}} \operatorname{erfc} \left(\frac{y}{2\sqrt{at}} + \right. \right. \\
 & \left. \left. \sqrt{(b+i\omega_1)t} \right) \right]
 \end{aligned} \tag{4.1.39}$$

$$g_1(y, t) = a_7f_3(y, t) + a_8f_4(y, t) + a_9f_5(y, t) \tag{4.1.40}$$

$$f_3(y, t) = \frac{e^{-a_3 t}}{2} \left[e^{-y \sqrt{\frac{1}{a}(b-a_3)}} \operatorname{erfc} \left(\frac{y}{2\sqrt{at}} - \sqrt{(b-a_3)t} \right) + e^{y \sqrt{\frac{1}{a}(b-a_3)}} \operatorname{erfc} \left(\frac{y}{2\sqrt{at}} + \sqrt{(b-a_3)t} \right) \right] \quad (4.1.41)$$

$$f_4(y, t) = \frac{1}{2} \left[e^{-y \sqrt{\frac{b}{a}}} \operatorname{erfc} \left(\frac{y}{2\sqrt{at}} - \sqrt{bt} \right) + e^{y \sqrt{\frac{b}{a}}} \operatorname{erfc} \left(\frac{y}{2\sqrt{at}} + \sqrt{bt} \right) \right] \quad (4.1.42)$$

$$f_5(y, t) = \frac{1}{2} \left[\left(t - \frac{y}{2\sqrt{ab}} \right) e^{-y \sqrt{\frac{b}{a}}} \operatorname{erfc} \left(\frac{y}{2\sqrt{at}} - \sqrt{bt} \right) + \left(t + \frac{y}{2\sqrt{ab}} \right) e^{y \sqrt{\frac{b}{a}}} \operatorname{erfc} \left(\frac{y}{2\sqrt{at}} + \sqrt{bt} \right) \right] \quad (4.1.43)$$

$$f_6(y, t) = \frac{e^{-a_6 t}}{2} \left[e^{-y \sqrt{\frac{1}{a}(b-a_6)}} \operatorname{erfc} \left(\frac{y}{2\sqrt{at}} - \sqrt{(b-a_6)t} \right) + e^{y \sqrt{\frac{1}{a}(b-a_6)}} \operatorname{erfc} \left(\frac{y}{2\sqrt{at}} + \sqrt{(b-a_6)t} \right) \right] \quad (4.1.44)$$

$$g_2(y, t) = a_7 f_7(y, t) + a_8 f_8(y, t) + a_9 f_9(y, t) \quad (4.1.45)$$

$$f_7(y, t) = \frac{e^{-a_3 t}}{2} \left[e^{-y \sqrt{Nr - Pra_3}} \operatorname{erfc} \left(\frac{y \sqrt{Pr}}{2\sqrt{t}} - \sqrt{\left(\frac{Nr}{Pr} - a_3 \right) t} \right) + e^{y \sqrt{Nr - Pra_3}} \operatorname{erfc} \left(\frac{y \sqrt{Pr}}{2\sqrt{t}} + \sqrt{\left(\frac{Nr}{Pr} - a_3 \right) t} \right) \right] \quad (4.1.46)$$

$$f_8(y, t) = \frac{1}{2} \left[e^{-y \sqrt{Nr}} \operatorname{erfc} \left(\frac{y \sqrt{Pr}}{2\sqrt{t}} - \sqrt{\frac{Nr}{Pr} t} \right) + e^{y \sqrt{Nr}} \operatorname{erfc} \left(\frac{y \sqrt{Pr}}{2\sqrt{t}} + \sqrt{\frac{Nr}{Pr} t} \right) \right] \quad (4.1.47)$$

$$f_9(y, t) = \frac{1}{2} \left[\left(t - \frac{y \sqrt{Pr}}{2\sqrt{Nr}} \right) e^{-y \sqrt{Nr}} \operatorname{erfc} \left(\frac{y \sqrt{Pr}}{2\sqrt{t}} - \sqrt{\frac{Nr}{Pr} t} \right) + \left(t + \frac{y \sqrt{Pr}}{2\sqrt{Nr}} \right) e^{y \sqrt{Nr}} \operatorname{erfc} \left(\frac{y \sqrt{Pr}}{2\sqrt{t}} + \sqrt{\frac{Nr}{Pr} t} \right) \right] \quad (4.1.48)$$

$$f_{10}(y, t) = \frac{1}{2} \left[e^{-y \sqrt{Kr Sc}} \operatorname{erfc} \left(\frac{y \sqrt{Sc}}{2\sqrt{t}} - \sqrt{Kr t} \right) + e^{y \sqrt{Kr Sc}} \operatorname{erfc} \left(\frac{y \sqrt{Sc}}{2\sqrt{t}} + \sqrt{Kr t} \right) \right] \quad (4.1.49)$$

$$f_{11}(y, t) = \frac{1}{2} \left[\left(t - \frac{y \sqrt{Sc}}{2\sqrt{Kr}} \right) e^{-y \sqrt{Sc Kr}} \operatorname{erfc} \left(\frac{y \sqrt{Sc}}{2\sqrt{t}} - \sqrt{Kr t} \right) + \left(t + \frac{y \sqrt{Sc}}{2\sqrt{Kr}} \right) e^{y \sqrt{Sc Kr}} \operatorname{erfc} \left(\frac{y \sqrt{Sc}}{2\sqrt{t}} + \sqrt{Kr t} \right) \right] \quad (4.1.50)$$

$$f_{12}(y, t) = \frac{e^{-a_6 t}}{2} \left[e^{-y\sqrt{Sc(Kr-a_6)}} \operatorname{erfc} \left(\frac{y\sqrt{Sc}}{2\sqrt{t}} - \sqrt{(Kr-a_6)t} \right) + e^{y\sqrt{Sc(Kr-a_6)}} \operatorname{erfc} \left(\frac{y\sqrt{Sc}}{2\sqrt{t}} + \sqrt{(Kr-a_6)t} \right) \right] \quad (4.1.51)$$

4.1.4.3 Nusselt number

The Nusselt number Nu can be written as

$$N_u = -\frac{\nu}{u_0(T-T_\infty)} \left(\frac{\partial T}{\partial y} \right)_{y=0} \quad (4.1.52)$$

It is obtained the Nusselt number from the equations (4.1.30) for ramped wall temperature is

$$N_u = -[h_{11}(t) - h_{11}(t-1)H(t-1)] \quad (4.1.53)$$

From the equation (4.1.34), it is obtained the Nusselt number for isothermal temperature is

$$N_u = -[h_{10}(t)] \quad (4.1.54)$$

4.1.4.4 Sherwood number:

Sherwood number is defined and denoted by the formula

$$s_h = -\left(\frac{\partial C}{\partial y} \right)_{y=0} \quad (4.1.55)$$

Using the equations (4.1.31) and (4.1.35), The Sherwood number for Ramped wall temperature and isothermal temperature can be written as,

$$s_h = -[h_{13}(t)] \quad (4.1.56)$$

4.1.4.5 Skin friction:

Expressions for skin-friction for both cases are calculated from Equations (4.1.32), (4.1.33), (4.1.36) and (4.1.37) using the relations

$$\tau^*(y, t) = -\mu\beta \left(1 + \frac{1}{\gamma} \right) \tau \quad (4.1.57)$$

$$\text{Where } \tau = \left. \frac{\partial u}{\partial y} \right|_{y=0} \quad (4.1.58)$$

For ramped wall temperature

$$\begin{aligned}\tau_{sin}(y, t) = & \frac{i}{2}h_1(t) - \frac{i}{2}h_2(t) + h_3(t) - h_3(y, t - 1)H(t - 1) + a_{10}h_5(t) + a_{11}h_6(t) + \\ & a_{12}h_7(t) - h_8(t) + h_8(t - 1)H(t - 1) - a_{10}h_{12}(t) - a_{11}h_{13}(t) - a_{12}h_{14}(t)\end{aligned}\quad (4.1.59)$$

$$\begin{aligned}\tau_{cos}(y, t) = & \frac{1}{2}h_1(t) + \frac{1}{2}h_2(t) + h_3(t) - h_3(y, t - 1)H(t - 1) + a_{10}h_5(t) + a_{11}h_6(t) + \\ & a_{12}h_7(t) - h_8(t) + h_8(t - 1)H(t - 1) - a_{10}h_{12}(t) - a_{11}h_{13}(t) - a_{12}h_{14}(t)\end{aligned}\quad (4.1.60)$$

For isothermal temperature

$$\begin{aligned}\tau_{sin}(y, t) = & \frac{i}{2}h_1(t) - \frac{i}{2}h_2(t) + (a_9 + a_{10})h_5(t) - a_9h_4(t) + a_{11}h_6(t) + a_{12}h_7(t) - \\ & a_9h_{10}(t) + a_9h_9(t) - a_{10}h_{12}(t) - a_{11}h_{13}(t) - a_{12}h_{14}(t)\end{aligned}\quad (4.1.61)$$

$$\begin{aligned}\tau_{cos}(y, t) = & \frac{1}{2}h_1(t) + \frac{1}{2}h_2(t) + (a_9 + a_{10})h_5(t) - a_9h_4(t) + a_{11}h_6(t) + a_{12}h_7(t) - \\ & a_9h_{10}(t) + a_9h_9(t) - a_{10}h_{12}(t) - a_{11}h_{13}(t) - a_{12}h_{14}(t)\end{aligned}\quad (4.1.62)$$

Where

$$h_1(t) = e^{-i\omega_1 t} \sqrt{\frac{b-i\omega_1}{a}} \operatorname{erf}(\sqrt{(b-i\omega_1)t}) + \frac{e^{-bt}}{\sqrt{\pi at}} \quad (4.1.63)$$

$$h_2(t) = e^{i\omega_1 t} \sqrt{\frac{b+i\omega_1}{a}} \operatorname{erf}(\sqrt{(b+i\omega_1)t}) + \frac{e^{-bt}}{\sqrt{\pi at}} \quad (4.1.64)$$

$$h_3(t) = a_7h_4(t) + a_8h_5(t) + a_9h_6(t) \quad (4.1.65)$$

$$h_4(t) = -e^{-a_3 t} \sqrt{\frac{b-a_3}{a}} \operatorname{erf}(\sqrt{(b-a_3)t}) + \frac{e^{-bt}}{\sqrt{\pi at}} \quad (4.1.66)$$

$$h_5(t) = -\sqrt{\frac{b}{a}} \operatorname{erf}(\sqrt{bt}) + \frac{e^{-bt}}{\sqrt{\pi at}} \quad (4.1.67)$$

$$h_6(t) = -\frac{1}{\sqrt{4ab}} \operatorname{erf}(\sqrt{bt}) - t \sqrt{\frac{b}{a}} \operatorname{erf}(\sqrt{bt}) + \frac{t e^{-bt}}{\sqrt{\pi at}} \quad (4.1.68)$$

$$h_7(t) = -e^{-a_6 t} \sqrt{\frac{b-a_6}{a}} \operatorname{erf}(\sqrt{(b-a_6)t}) + \frac{e^{-bt}}{\sqrt{\pi at}} \quad (4.1.69)$$

$$h_8(t) = a_7h_9(t) + a_8h_{10}(t) + a_9h_{11}(t) \quad (4.1.70)$$

$$h_9(t) = -e^{-a_3 t} \sqrt{Nr - Pr a_3} \operatorname{erf}\left(\sqrt{\left(\frac{Nr}{Pr} - a_3\right) t}\right) + \sqrt{\frac{Pr}{\pi t}} e^{-\frac{Nr}{Pr} t} \quad (4.1.71)$$

$$h_{10}(t) = -\sqrt{Nr} \operatorname{erf}\left(\sqrt{\frac{Nr}{Pr} t}\right) + \sqrt{\frac{Pr}{\pi t}} e^{-\frac{Nr}{Pr} t} \quad (4.1.72)$$

$$h_{11}(t) = -\frac{Pr}{2\sqrt{Nr}} \operatorname{erf}\left(\sqrt{\frac{Nr}{Pr} t}\right) - \sqrt{Nr} t \operatorname{erf}\left(\sqrt{\frac{Nr}{Pr} t}\right) + \sqrt{\frac{t Pr}{\pi}} e^{-\frac{Nr}{Pr} t} \quad (4.1.73)$$

$$h_{12}(t) = -\sqrt{Kr Sc} \operatorname{erf}(\sqrt{Kr t}) + \sqrt{\frac{Sc}{\pi t}} e^{-Kr t} \quad (4.1.74)$$

$$h_{13}(t) = -\sqrt{\frac{Sc}{4 Kr}} \operatorname{erf}(\sqrt{Kr t}) - t\sqrt{Sc Kr} \operatorname{erf}(\sqrt{Kr t}) + \sqrt{\frac{t Sc}{\pi}} e^{-Kr t} \quad (4.1.75)$$

$$h_{14}(t) = -e^{-a_6 t} \sqrt{Sc(Kr - a_6)} \operatorname{erf}(\sqrt{(Kr - a_6) t}) + \sqrt{\frac{Sc}{\pi t}} e^{-Kr t} \quad (4.1.76)$$

4.1.5 Results and Discussion

In order to get a clear insight of the physics of the problem, a parametric study is performed and the obtained numerical results are explained with the help of graphical illustrations. The non-dimensional fluid velocity, fluid temperature and concentration profiles are analysed for several values of different physical parameters in Figures (4.1.2) to (4.1.12). The influence of Casson fluid parameter γ on velocity profiles is shown in Figure 4.1.2. It is found that velocity increase with increasing value of γ . It is important to note that an increase in Casson parameter makes the velocity boundary layer thickness shorter. It is further observed from this graph, when the Casson parameter γ is large enough, the non-Newtonian behaviours disappear and the fluid purely behaves like a Newtonian fluid. In Figure 4.1.3, velocity profiles have been plotted for various values of permeability parameter k by keeping other parameters fixed. It is observed that for large values of k , velocity and boundary layer thickness increase which explains the physical situation that as k increases, the resistance of the porous medium is dropped which increases the motion of the flow regime, ultimately enhancing the velocity field. Figure 4.1.4 displays the velocity and boundary layer thickness decreases when M is increased. Physically, it may also be predictable due to the fact that the application of resistive type force (called Lorentz force) similar to the drag force. Figure 4.1.5 and Figure 4.1.6 shows effect of thermal radiation parameter Nr on velocity and temperature

profiles for different values of y for both thermal plates. It is seen that, thermal radiation parameter tends to reduced velocity and temperature profiles.

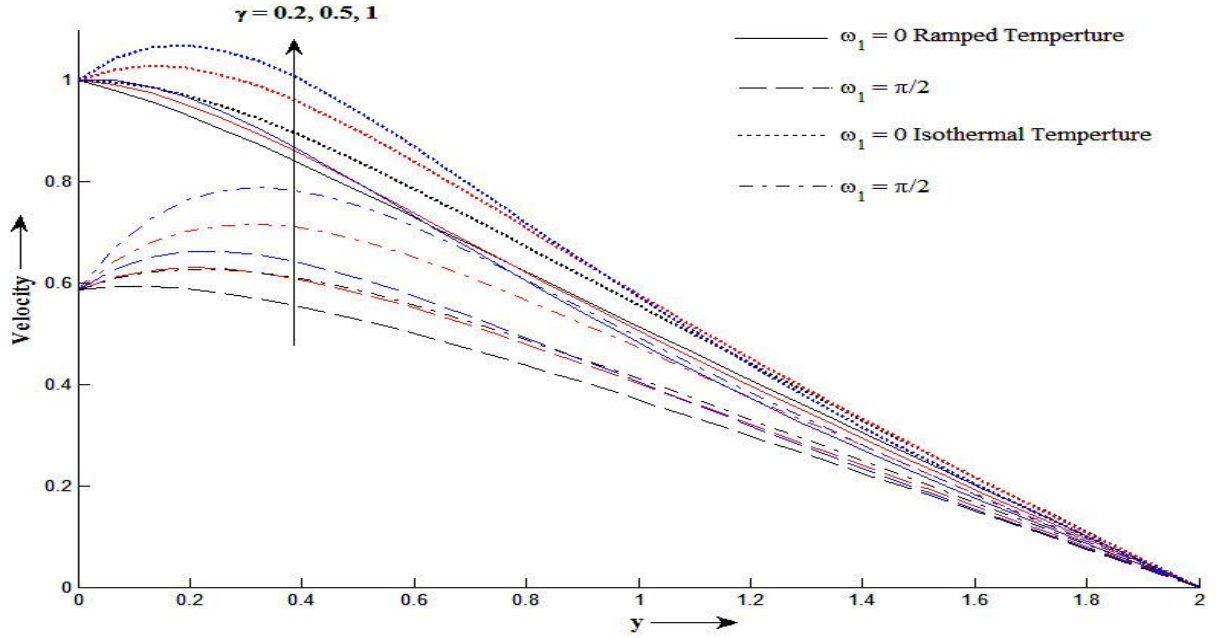


Figure 4.1.2: Velocity profile u for different values of y and γ at $M = 0.5, Sc = 0.6, Gm = 5, Gr = 10, Pr = 7, k = 1, t = 0.6, Nr = 0.5$ and $Kr = 2$.

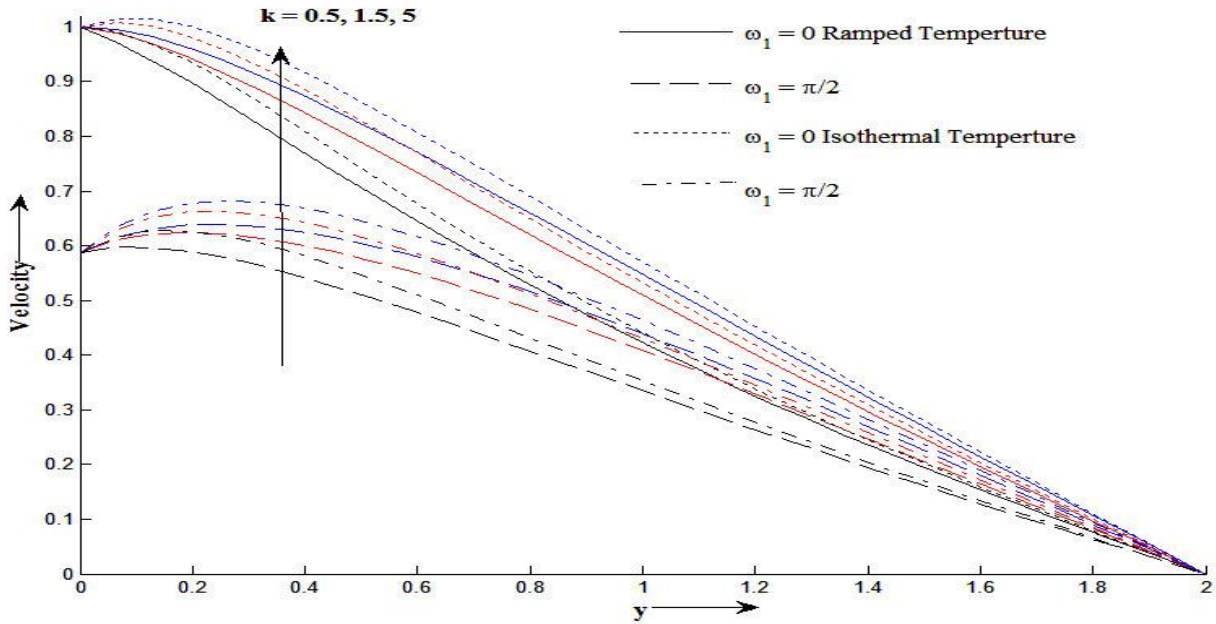


Figure 4.1.3: Velocity profile u for different values of y and k at $M = 0.5, Sc = 0.6, Gm = 5, Gr = 10, Pr = 25, \gamma = 0.6, t = 0.6, Nr = 0.5$ and $Kr = 2$

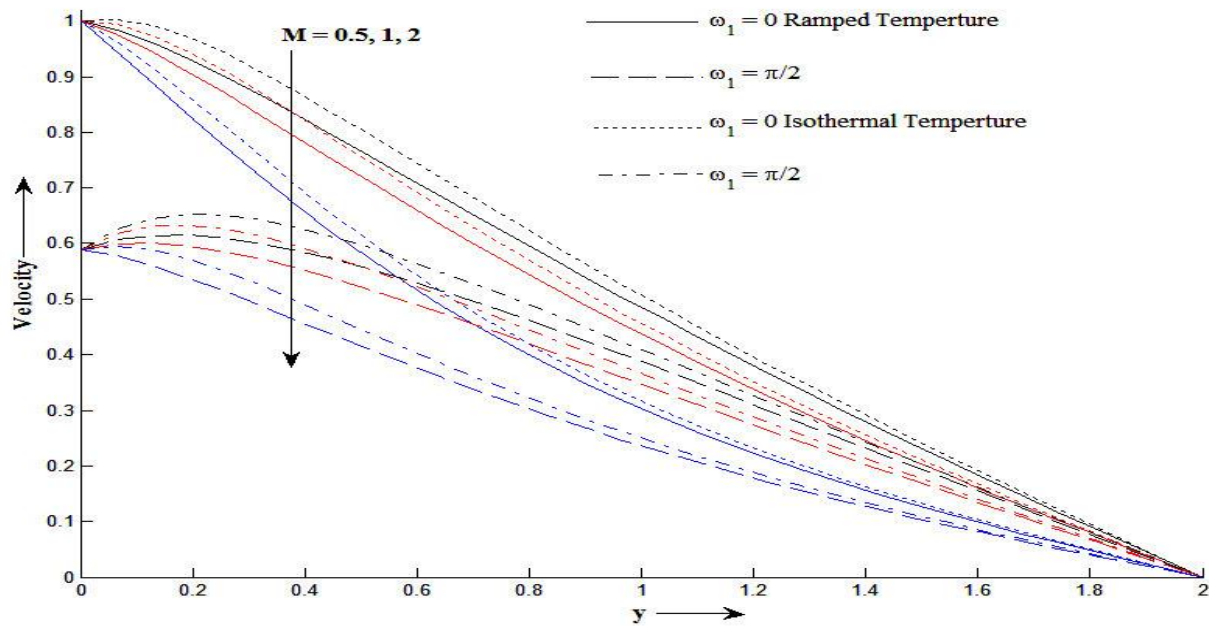


Figure 4.1.4: Velocity profile u for different values of y and M at $k = 1, Sc = 0.6, Gm = 5, Gr = 10, Pr = 25, \gamma = 0.6, t = 0.6, Nr = 0.5$ and $Kr = 2$.

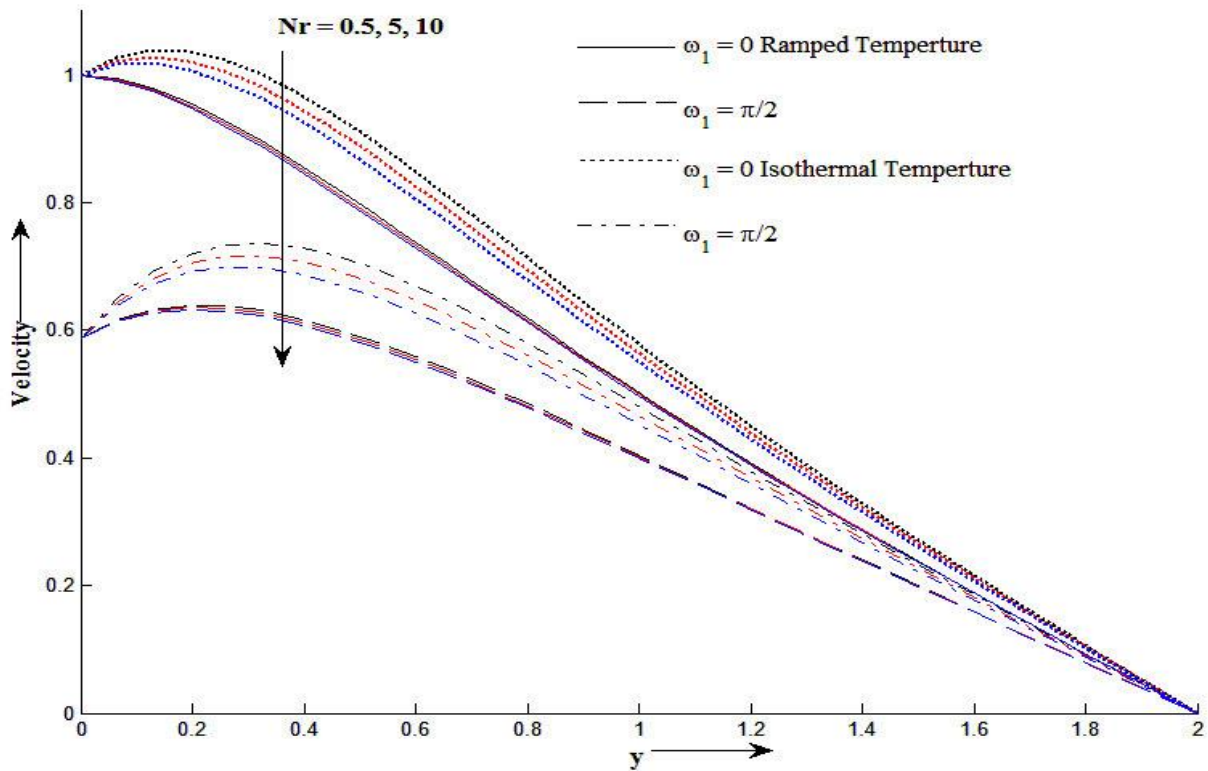


Figure 4.1.5: Velocity profile u for different values of y and Nr at $k = 1, Sc = 0.6, Gm = 5, Gr = 10, Pr = 7, \gamma = 0.6, t = 0.6, M = 0.5$ and $Kr = 2$.

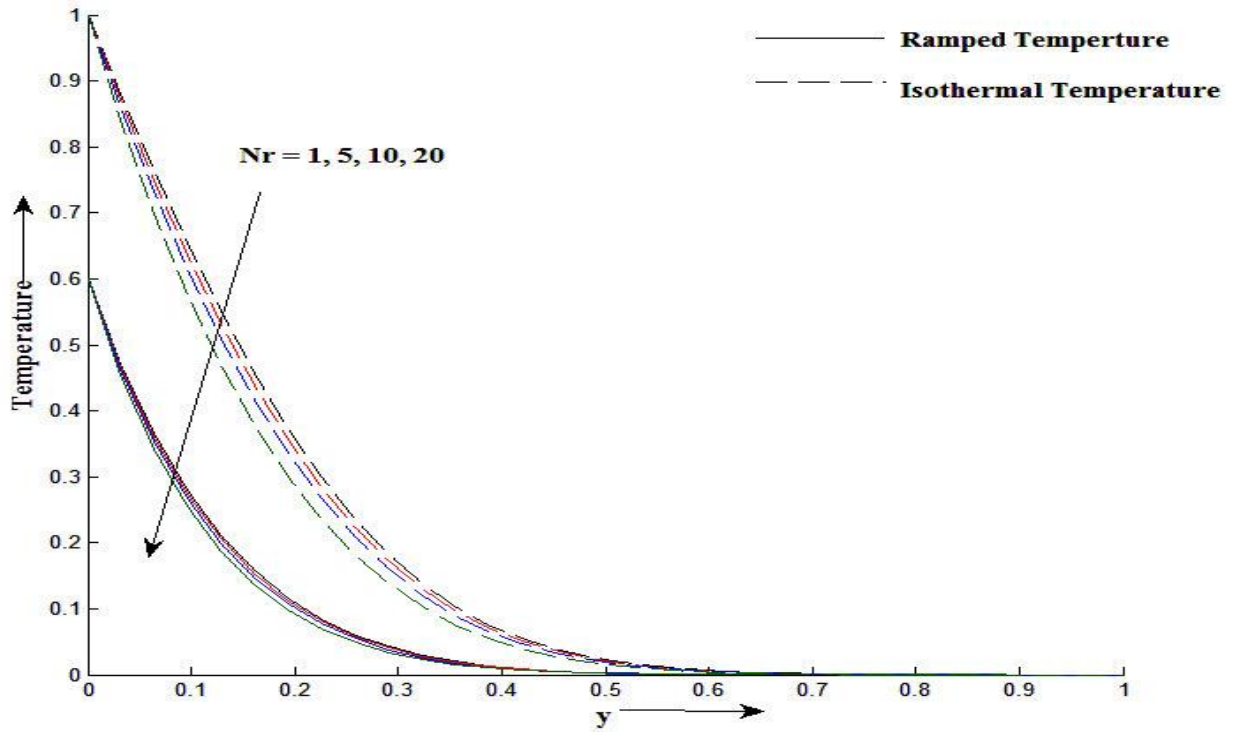


Figure 4.1.6: Temperature profile θ for different values of y and Nr at $t = 0.6$ and $Pr = 25$

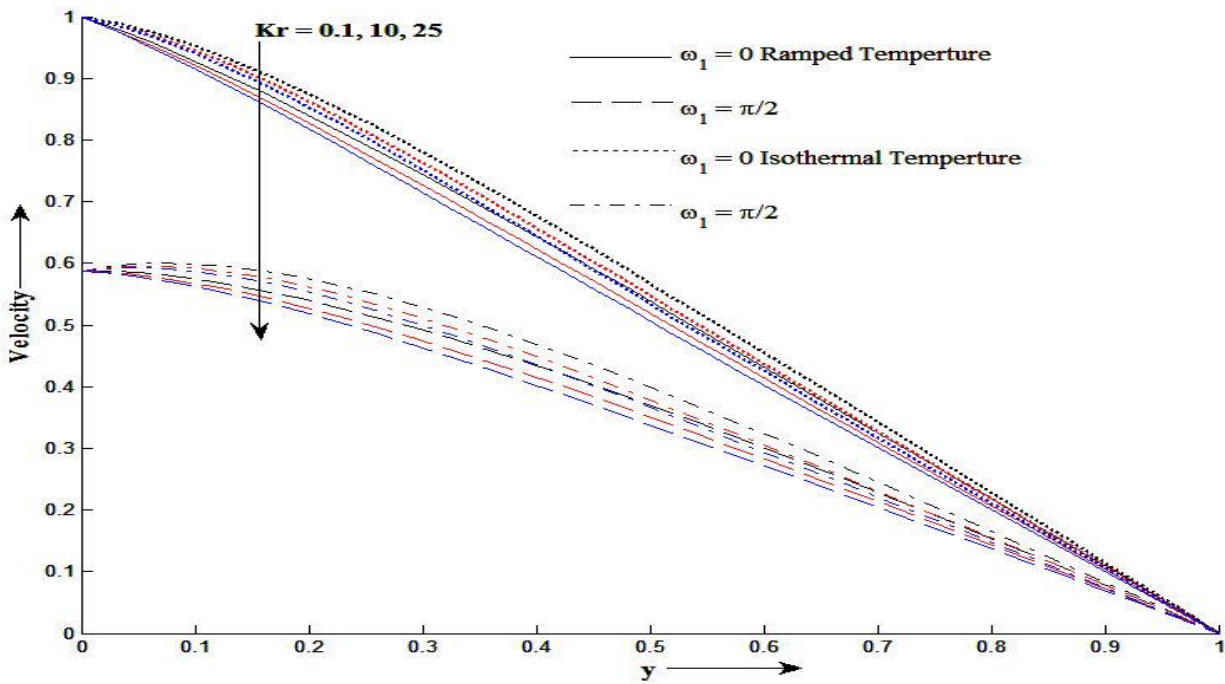


Figure 4.1.7: Velocity profile u for different values of y and Kr at $k = 1, Sc = 0.6, Gm = 5, Gr = 10, Pr = 25, \gamma = 0.6, t = 0.6, M = 0.5$ and $Nr = 0.5$.

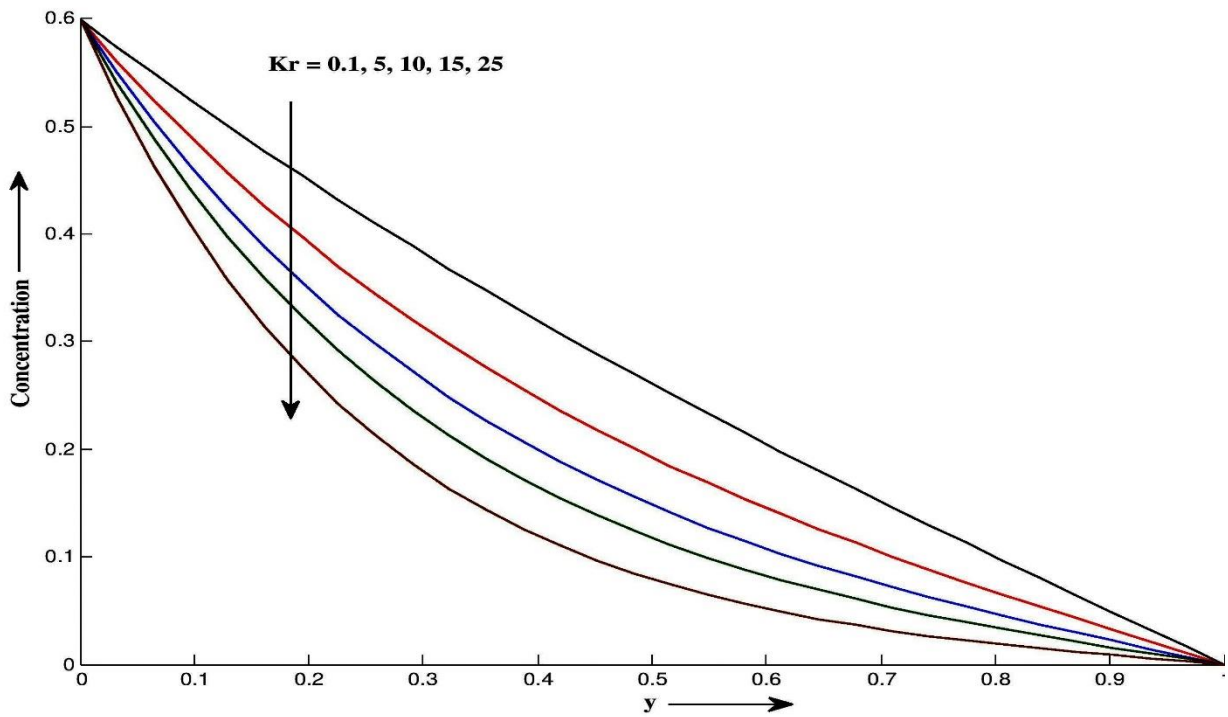


Figure 4.1.8: Concentration profile C for different values of y and Kr at $Sc = 0.6$ and $t = 0.6$

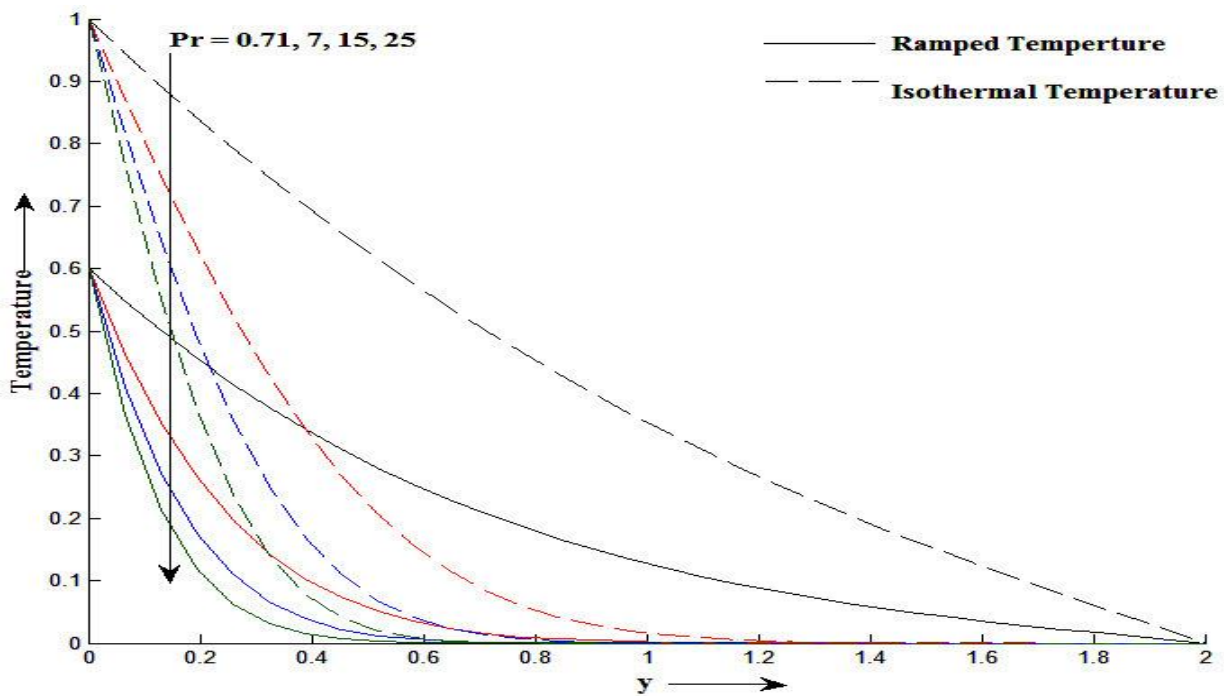


Figure 4.1.9: Temperature profile θ for different values of y and Pr at $t = 0.6$ and $Nr = 0.5$

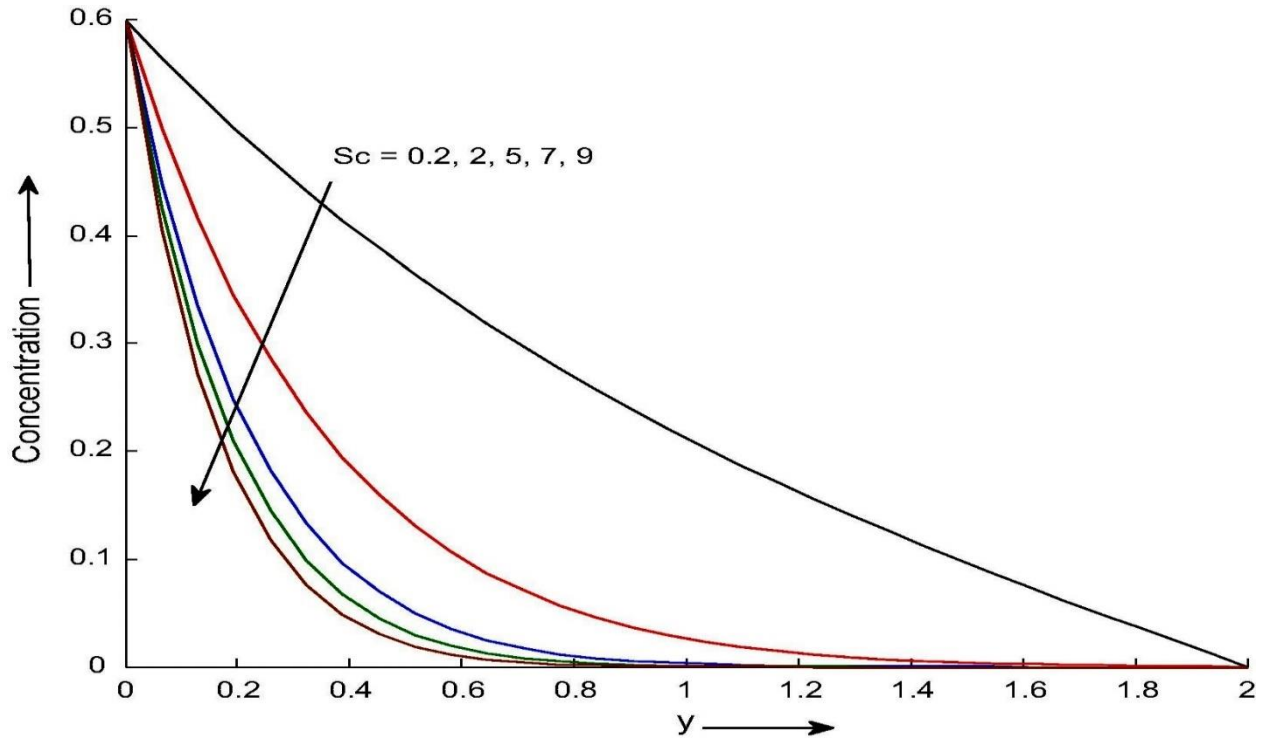


Figure 4.1.10: Concentration profile C for different values of y and Sc at $Kr = 2$ and $t = 0.6$

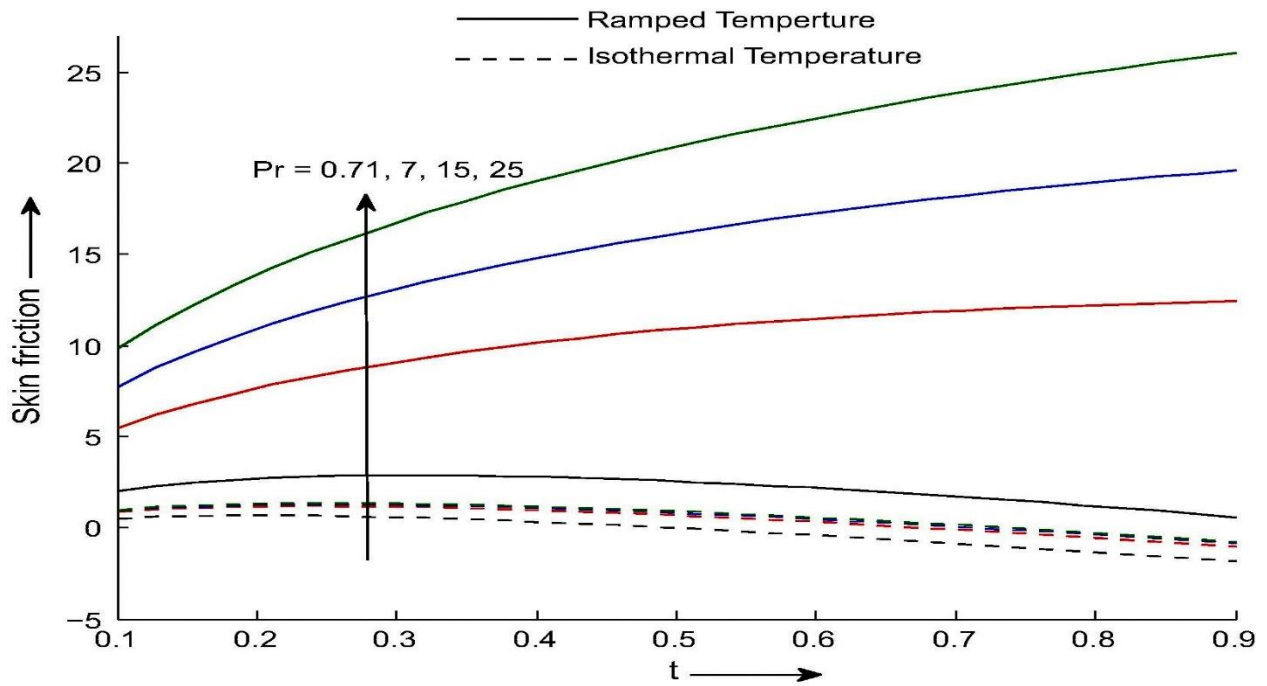


Figure 4.1.11: Skin friction for different values of t and Pr at $k = 1, Sc = 0.6, Gm = 5, Gr = 2, Nr = 0.5, Kr = 1, \gamma = 0.1$ and $M = 0.5$

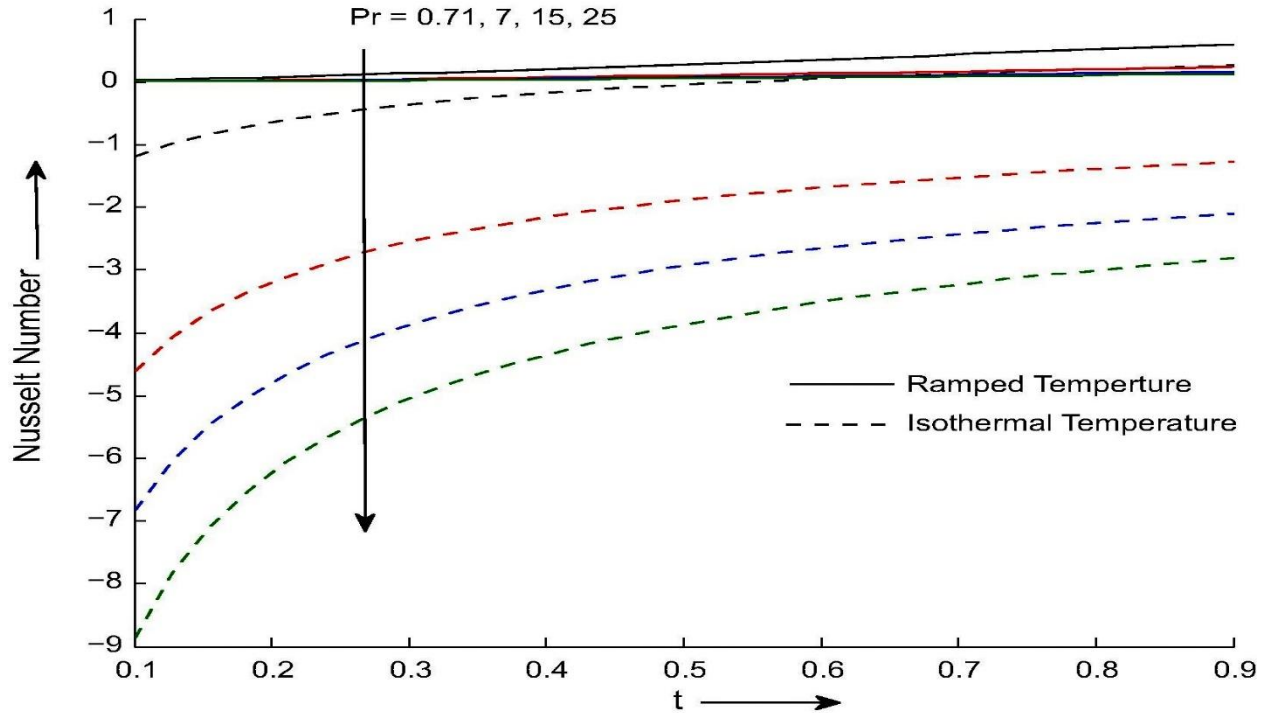


Figure 4.1.12: Nusselt number for different values of t and Pr at $k = 1, Sc = 0.6, Gm = 5,$

$$Gr = 2, Kr = 1, \gamma = 0.1, Nr = 0.5 \text{ and } M = 0.5.$$

If dimensionless quantity $Nr = \frac{16 a^* \sigma^* v^2 T'_{\infty}{}^3}{k_4 U_0^2}$ instead of $Nr = -\frac{16 a^* \sigma^* v^2 T'_{\infty}{}^3}{k_4 U_0^2}$ is considered in energy equation 4.1.9 then motion of the fluid and heat transfer process increase with increase in Nr . Physically, Due to increasing thermal radiation parameter Nr , heat is generated in fluid flow, which leads to improvement in heat transfer as well as momentum throughout the fluid flow region. Figure 4.1.7 and Figure 4.1.8 depict that velocity and concentration profiles for different values of chemical reaction parameter Kr by keeping other parameters fixed. It is evident that, velocity and concentration profiles decreases with increase in Kr . This graphical behaviour of velocity and concentration is in good agreement with physical point of view of the fluid flow phenomena. It is depicted from Figure 4.1.9 that, the temperature decreases as the Prandtl number Pr increases. It is justified due to the fact that thermal conductivity of the fluid decreases with increasing Prandtl number Pr and hence decreases the thermal boundary layer thickness. It is depicted from Figure 4.1.10 that, concentration decreases with increasing values of Sc . Figure 4.1.11 exhibits the Skin friction for different values of Pr . It is seen that, Skin friction increases with increase in Pr . Skin friction is more for ramped wall temperature compared to isothermal temperature. Figure 4.1.12 shows effect of Pr on Nusselt number. It is seen that Nusselt number decrease tendency with Pr .

Table 4.1.1: Skin friction variation for air ($Pr = 0.71$ and $\sin \omega_1 t = 0$)

t	γ	Sc	Gr	Gm	Nr	Kr	M	k	Skin friction τ for Ramped temperature	Skin friction τ for isothermal temperature
0.4	0.1	0.6	2	5	0.5	1	0.5	1	2.7934	0.3121
0.4	0.2	0.6	2	5	0.5	1	0.5	1	2.8531	0.2179
0.4	0.3	0.6	2	5	0.5	1	0.5	1	3.0731	0.0556
0.4	0.1	0.7	2	5	0.5	1	0.5	1	2.7197	0.2383
0.4	0.1	0.8	2	5	0.5	1	0.5	1	2.6561	0.1747
0.4	0.1	0.6	3	5	0.5	1	0.5	1	3.4741	-0.2479
0.4	0.1	0.6	5	5	0.5	1	0.5	1	4.8355	-1.3679
0.4	0.1	0.6	2	7	0.5	1	0.5	1	3.3663	0.8849
0.4	0.1	0.6	2	9	0.5	1	0.5	1	3.9391	1.4577
0.4	0.1	0.6	2	5	0.7	1	0.5	1	2.0626	0.3399
0.4	0.1	0.6	2	5	0.8	1	0.5	1	1.8636	0.3533
0.4	0.1	0.6	2	5	0.5	0.9	0.5	1	2.4719	-0.0095
0.4	0.1	0.6	2	5	0.5	0.8	0.5	1	1.7080	-0.7733
0.4	0.1	0.6	2	5	0.5	1	0.7	1	2.9362	0.2960
0.4	0.1	0.6	2	5	0.5	1	0.9	1	3.0545	0.1787
0.4	0.1	0.6	2	5	0.5	1	0.5	1.1	2.7289	0.3044
0.4	0.1	0.6	2	5	0.5	1	0.5	1.2	2.6711	0.2928
0.5	0.1	0.6	2	5	0.5	1	0.5	0.5	2.5466	-0.0261
0.6	0.1	0.6	2	5	0.5	1	0.5	0.5	2.1748	-0.4287

Table 4.1.2: Skin friction variation for water ($Pr = 7$ and $\sin \omega_1 t = 0$)

t	γ	Sc	Gr	Gm	Nr	Kr	M	k	Skin friction τ for Ramped temperature	Skin friction τ for isothermal temperature
0.4	0.1	0.6	2	5	0.5	1	0.5	1	10.1279	0.9596
0.4	0.2	0.6	2	5	0.5	1	0.5	1	12.4865	0.7843
0.4	0.3	0.6	2	5	0.5	1	0.5	1	16.2812	0.5758
0.4	0.1	0.7	2	5	0.5	1	0.5	1	10.0541	0.8858
0.4	0.1	0.8	2	5	0.5	1	0.5	1	9.9906	0.8223
0.4	0.1	0.6	3	5	0.5	1	0.5	1	14.4758	0.7234

0.4	0.1	0.6	5	5	0.5	1	0.5	1	23.1716	0.2509
0.4	0.1	0.6	2	7	0.5	1	0.5	1	10.7007	1.5324
0.4	0.1	0.6	2	9	0.5	1	0.5	1	11.2735	2.1053
0.4	0.1	0.6	2	5	0.7	1	0.5	1	7.0476	0.9612
0.4	0.1	0.6	2	5	0.8	1	0.5	1	6.1810	0.9620
0.4	0.1	0.6	2	5	0.5	0.9	0.5	1	9.8063	0.6381
0.4	0.1	0.6	2	5	0.5	0.8	0.5	1	9.0425	-0.1258
0.4	0.1	0.6	2	5	0.5	1	0.7	1	10.6974	0.9367
0.4	0.1	0.6	2	5	0.5	1	0.9	1	11.4713	0.8105
0.4	0.1	0.6	2	5	0.5	1	0.5	1.1	9.9141	0.9546
0.4	0.1	0.6	2	5	0.5	1	0.5	1.2	9.7365	0.9452
0.5	0.1	0.6	2	5	0.5	1	0.5	1	10.8952	0.6697
0.6	0.1	0.6	2	5	0.5	1	0.5	1	11.4679	0.3041

Table 4.1.3: Skin friction variation for ($Pr = 25$ and $\sin \omega_1 t = 0$)

t	γ	Sc	Gr	Gm	Nr	Kr	M	k	Skin friction τ for Ramped temperature	Skin friction τ for isothermal temperature
0.4	0.1	0.6	2	5	0.5	1	0.5	1	19.0090	1.1659
0.4	0.2	0.6	2	5	0.5	1	0.5	1	24.2296	0.9779
0.4	0.3	0.6	2	5	0.5	1	0.5	1	32.4505	0.7616
0.4	0.1	0.7	2	5	0.5	1	0.5	1	18.9352	1.0922
0.4	0.1	0.8	2	5	0.5	1	0.5	1	18.8716	1.0286
0.4	0.1	0.6	3	5	0.5	1	0.5	1	27.7974	1.0329
0.4	0.1	0.6	5	5	0.5	1	0.5	1	45.3743	0.7667
0.4	0.1	0.6	2	7	0.5	1	0.5	1	19.5818	1.7388
0.4	0.1	0.6	2	9	0.5	1	0.5	1	20.1546	2.3116
0.4	0.1	0.6	2	5	0.7	1	0.5	1	12.9509	1.1662
0.4	0.1	0.6	2	5	0.8	1	0.5	1	11.2459	1.1663
0.4	0.1	0.6	2	5	0.5	0.9	0.5	1	18.6874	0.8444
0.4	0.1	0.6	2	5	0.5	0.8	0.5	1	17.9236	0.0805
0.4	0.1	0.6	2	5	0.5	1	0.7	1	20.1065	1.1420
0.4	0.1	0.6	2	5	0.5	1	0.9	1	21.6913	1.0147

0.4	0.1	0.6	2	5	0.5	1	0.5	1.1	18.6104	1.1613
0.4	0.1	0.6	2	5	0.5	1	0.5	1.2	18.2847	1.1522
0.5	0.1	0.6	2	5	0.5	1	0.5	1	20.8744	0.8981
0.6	0.1	0.6	2	5	0.5	1	0.5	1	22.4534	0.5518

Table 4.1.4: Nusselt number variation for air ($Pr = 0.71$)

t	Nr	Nusselt number Nu for Ramped Temperature	Nusselt number Nu for isothermal Temperature
0.4	0.5	0.2026	-0.1803
0.4	0.7	0.2721	0.0166
0.4	0.8	0.3047	0.1092
0.5	0.5	0.2758	-0.0495
0.6	0.5	0.3534	0.0518

Table 4.1.5: Nusselt number variation for water ($Pr = 7$)

t	Nr	Nusselt number Nu for Ramped Temperature	Nusselt number Nu for isothermal Temperature
0.4	0.5	0.0711	-2.1601
0.4	0.7	0.0991	-2.0813
0.4	0.8	0.1130	-2.0422
0.5	0.5	0.0991	-1.8879
0.6	0.5	0.1299	-1.6834

Table 4.1.6: Nusselt number variation for ($Pr = 25$)

t	Nr	Nusselt number Nu for Ramped Temperature	Nusselt number Nu for isothermal Temperature
0.4	0.5	0.0379	-4.3536
0.4	0.7	0.0530	-4.3111
0.4	0.8	0.0606	-4.2899
0.5	0.5	0.0530	-3.8702
0.6	0.5	0.0696	-3.5113

Table 4.1.7: Sherwood number variation

t	Kr	Sc	Sherwood number Sh
0.4	1	0.6	0.2532
0.4	1.1	0.6	0.2745
0.4	1.2	0.6	0.2952
0.4	1	0.7	0.2734
0.4	1	0.8	0.2923
0.5	1	0.6	0.3414
0.6	1	0.6	0.4334

The variation of the Nusselt number, Skin friction and Sherwood number for air ($Pr = 0.71$), water ($Pr = 7$) and ($Pr = 25$) are shown in Tables (4.1.1) to (4.1.7) for various values of the governing parameters. Skin friction increases in ramped wall temperature while decrease in isothermal temperature with increase in γ , Gr and M . Skin friction decreases in case of ramped wall temperature while increase in isothermal temperature with increase in Nr . For both thermal cases, Skin friction decreases with increase in Sc and k while Skin friction increases with increase in Gm and Kr . Nusselt number increases with increase in Nr and t . Sherwood number increases with increase in Kr , Sc and t . Effect of all parameters γ , Gr , M , Nr , Sc , k , Gm and Kr on Skin friction and Nusselt number are similar in air and water. For air, Skin friction decreases with increase in t . For water, Skin friction increases in a Ramped wall temperature while decreases in isothermal temperature with increase in t . From Table 4.1.1 to Table 4.1.6, it is observed that Magnitude of Skin friction and Nusselt number increases with increase in Pr . It is seen that magnitude of Skin friction and Nusselt number is more for Casson fluid compared with water and air.

4.1.6 Conclusion

Concluding remarks can be summarized as follows:

- The fluid velocity decreases with increase in magnetic parameter M and chemical reaction parameter Kr .
- Permeability of porous medium k , Casson fluid parameter γ and positive values of thermal radiation Nr tends to improved motion of the fluid flow throughout the flow field.

- Temperature decreases as the Prandtl number Pr
- Schmidt number Sc and chemical reaction parameter Kr tends retard effects in mass transfer process.
- Skin friction increases while Nusselt number decreases with increase in Pr .
- Sherwood number increases with increase in Kr , Sc and t .

4.2 SECTION II: EFFECTS OF THERMAL RADIATION AND CHEMICAL REACTION ON MHD CASSON FLUID FLOW PAST OVER AN EXPONENTIALLY ACCELERATED VERTICAL PLATE EMBEDDED IN POROUS MEDIUM

In this Section, it is considered the effects of thermal radiation and chemical reaction on the unsteady MHD flow of Casson fluid past an exponentially moving vertical plate with ramped wall temperature and ramped surface concentration. The fluid is electrically conducting and passing through a porous medium. This phenomenon is modelled in the form of partial differential equations with initial and boundary conditions. The governing dimensionless equations are solved using the Laplace transform technique and analytical expressions for velocity, temperature and concentration profiles are obtained. In order to understand effects of ramped temperature with ramped surface concentration, obtained results are compared with that of isothermal temperature with ramped surface concentration.

4.2.1 Introduction of the problem

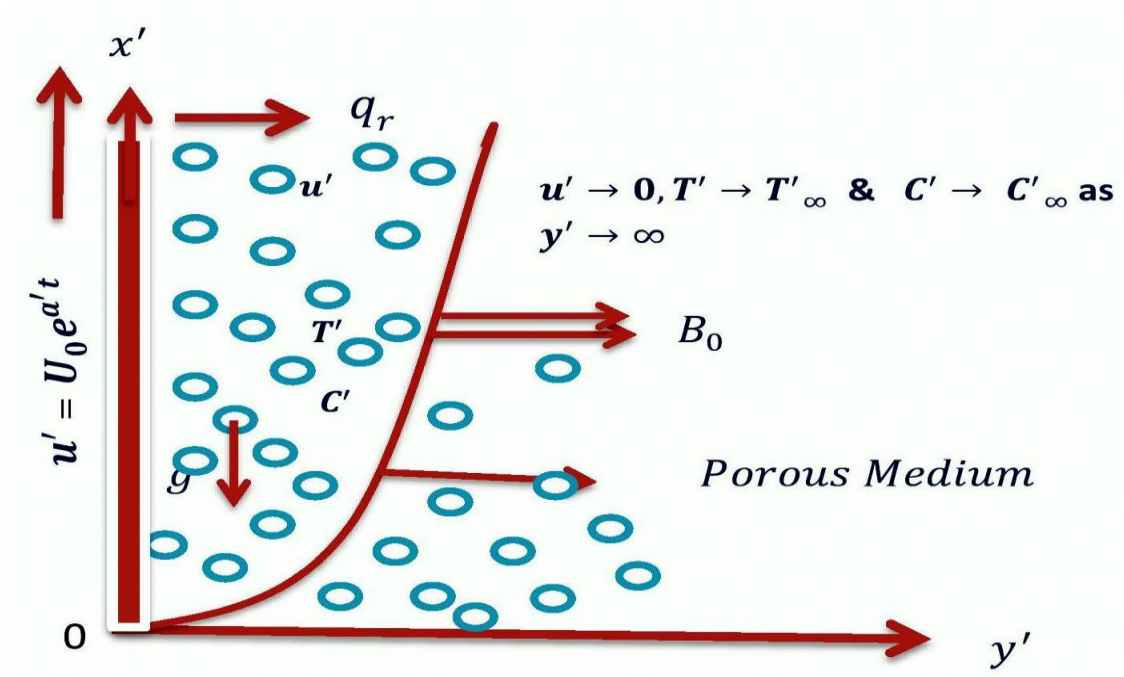
To extend research work of previous section, it is proposed to study the effects of chemical reaction and thermal radiation effects on MHD Casson fluid flow past an exponentially accelerated plate with ramped wall temperature and ramped surface concentration through porous medium. Free convection effects on MHD flow past an exponentially accelerated plate was studied by Singh and Kumar [161]. Recently, Pramanik [31] studied thermal radiation effects on Casson fluid flow and heat transfer past an exponentially porous stretching surface. Nadeem et al. [46] considered MHD flow of a Casson fluid over an exponentially shrinking sheet. Muthucumaraswamy et al. [78] studied mass transfer effects on exponentially accelerated isothermal vertical plate. Raju et al. [119] discussed MHD flow over an exponentially moving plate with heat absorption.

Prominence of porous medium in MHD flow is presented by Ali et al. [86]. Recently, Kataria and Patel [110] obtained analytical solution of MHD Casson fluid flow with radiation and reaction through embedded porous medium. However, all researchers considered ramped temperature with ramped surface concentration profiles, it is to be noted that interval for ramped profile varies from material to material depending upon the specific heat and mass transfer capacity of the material. Seth et al. [141] considered the problems of MHD flow with ramped wall temperature, whereas Seth [148] considered MHD flow with chemically reacting fluid past an accelerated moving vertical plate with ramped boundary conditions in porous medium.

4.2.2 Novelty of the Problem

Aim of this investigation is to study of unsteady free convective MHD flow of radiating and chemically reacting Casson fluid past an exponentially accelerated plate through embedded porous medium when plate has a ramped temperature with ramped surface concentration. Further, the expressions for the temperature gradient, concentration gradient and skin friction have been derived.

4.2.3 Mathematical Formulation of the Problem



$$T' = \begin{cases} T'_{\infty} + (T'_{\infty} - T'_{\infty}) t'/t_0 & \text{if } 0 < t' < t_0 \\ T'_{\infty} & \text{if } t' \geq t_0 \end{cases}, C' = \begin{cases} C'_{\infty} + (C'_{\infty} - C'_{\infty}) t'/t_0 & \text{if } 0 < t' < t_0 \\ C'_{\infty} & \text{if } t' \geq t_0 \end{cases}; y' = 0$$

Figure 4.2.1: Physical sketch of the Problem

As shown in Figure 4.2.1, x' – axis is along the wall and y' – axis is normal to it. A uniform magnetic field B_0 is applied along y' - direction. Initially, at time $t' \leq 0$, both the fluid and the plate are at rest with constant temperature T'_{∞} and the concentration at the surface is C'_{∞} respectively. At time $t' > 0$, the plate is exponentially accelerated in the vertical direction against gravitational field with velocity $U_0 e^{\alpha t}$, the temperature of the plate is either raised or lowered to $T'_{\infty} + (T'_{\infty} - T'_{\infty}) t'/t_0$ when $t' \leq t_0$, for $t' > t_0$, which is maintained at the constant temperature T'_{∞} . The

level of mass transfer at the surface of the wall is either raised or lowered to $C'_\infty + (C'_w + C'_\infty) t'/t_0$ when $t' \leq t_0$, for $t' > t_0$, which is maintained constant surface concentration C'_w respectively.

It is assumed that, the flow of fluid is confined in one dimensional incompressible, whereas induce magnetic field, electric field and viscous dissipation term in the energy equation is neglected. Under above assumptions and Boussinesq's approximation, governing equations are given below:

$$\rho \frac{\partial u'}{\partial t'} = \mu\beta \left(1 + \frac{1}{\gamma}\right) \frac{\partial^2 u'}{\partial y'^2} - \sigma B_0^2 u' - \frac{\mu\phi}{k'} u' + \rho g\beta'_T (T' - T'_\infty) + \rho g\beta'_C (C' - C'_\infty) \quad (4.2.1)$$

$$\frac{\partial T'}{\partial t'} = \frac{k_4}{\rho c_p} \frac{\partial^2 T'}{\partial y'^2} - \frac{1}{\rho c_p} \frac{\partial q_r}{\partial y'} \quad (4.2.2)$$

$$\frac{\partial C'}{\partial t'} = D_M \frac{\partial^2 C'}{\partial y'^2} - k'_2 (C' - C'_\infty) \quad (4.2.3)$$

with following initial and boundary conditions:

$$u' = 0, \quad T' = T'_\infty, \quad C' = C'_\infty; \text{ as } y' \geq 0 \text{ and } t' \leq 0$$

$$u' = U_0 e^{a't} \text{ as } t' > 0 \text{ and } y' = 0, \quad T' = \begin{cases} T'_\infty + (T'_w - T'_\infty) t'/t_0 & \text{if } 0 < t' < t_0 \\ T'_w & \text{if } t' \geq t_0 \end{cases},$$

$$C' = \begin{cases} C'_\infty + (C'_w - C'_\infty) t'/t_0 & \text{if } 0 < t' < t_0 \\ C'_w & \text{if } t' \geq t_0 \end{cases}; y' = 0$$

$$u' \rightarrow 0, T' \rightarrow T'_\infty, \quad C' \rightarrow C'_\infty; \text{ as } y' \rightarrow \infty \text{ and } t' \geq 0 \quad (4.2.4)$$

Using the Rosseland [91], the radiative heat flux term is given by.

$$q_r' = -\frac{4\sigma^*}{3k^*} \frac{\partial T'^4}{\partial y'} \quad (4.2.5)$$

Where σ^* and k^* are Stefan Boltzmann constant and mean absorption coefficient respectively. Assuming that the temperature difference between the fluid within the boundary layer and free stream is small, so T'^4 can be expressed as a linear combination of the temperature, using Taylor's series, expand T'^4 about T'_∞ and neglecting higher order terms.

$$T'^4 \cong 4T'^3_\infty T' - 3T'^4_\infty \quad (4.2.6)$$

$$\frac{\partial q_r'}{\partial y'} = -\frac{16\sigma^* T_\infty'^3}{3k^*} \frac{\partial^2 T'}{\partial y'^2} \quad (4.2.7)$$

Using equations (4.2.7) and (4.2.6) in equation (4.2.5),

$$\frac{\partial T'}{\partial t'} = \frac{k_4}{\rho c_p} \frac{\partial^2 T'}{\partial y'^2} + \frac{1}{\rho c_p} \frac{16\sigma^* T_\infty'^3}{3k^*} \frac{\partial^2 T'}{\partial y'^2} \quad (4.2.8)$$

Introducing the following dimensionless quantities:

$$y = \frac{U_0 y'}{v}, u = \frac{u'}{U_0}, t = \frac{t' U_0^2}{v}, \theta = \frac{(T' - T'_\infty)}{(T'_w - T'_\infty)}, C = \frac{(C' - C'_\infty)}{(C'_w - C'_\infty)}$$

In the equations (4.2.1) to (4.2.4) dropping out the " ' " notation (for simplicity),

$$\frac{\partial u}{\partial t} = \left(1 + \frac{1}{\gamma}\right) \frac{\partial^2 u}{\partial y^2} - \left(M^2 + \frac{1}{k}\right) u + Gr \theta + Gm C \quad (4.2.9)$$

$$\frac{\partial \theta}{\partial t} = \frac{1 + Nr}{Pr} \frac{\partial^2 \theta}{\partial y^2} \quad (4.2.10)$$

$$\frac{\partial C}{\partial t} = \frac{1}{Sc} \frac{\partial^2 C}{\partial y^2} - Kr C \quad (4.2.11)$$

with initial and boundary condition

$$u = \theta = C = 0, \quad y \geq 0, t = 0$$

$$u = e^{a't}, \theta = \begin{cases} t, & 0 < t \leq 1 \\ 1, & t > 1 \end{cases} = tH(t) - (t-1)H(t-1),$$

$$C = \begin{cases} t, & 0 < t \leq 1 \\ 1, & t > 1 \end{cases} = tH(t) - (t-1)H(t-1), \quad y = 0, \quad t > 0$$

$$u \rightarrow 0, \theta \rightarrow 0, C \rightarrow 0 \quad \text{as } y \rightarrow \infty, t > 0 \quad (4.2.12)$$

where, H(.) is Heaviside unit step function.

$$Gr = \frac{g v \beta'_T (T'_w - T'_\infty)}{U_0^3}, M^2 = \frac{\sigma B_0^2 v}{\rho U_0^2}, Gm = \frac{v g \beta'_C (C'_w - C'_\infty)}{U_0^3}, Pr = \frac{\rho v c_p}{k_4}, Nr = \frac{16\sigma^* T_\infty'^3}{3k_4 k^*}, Sc = \frac{v}{D_M},$$

$$\frac{1}{k} = \frac{v \phi^2}{k' U_0^2}, Kr = \frac{v k'_2}{U_0^2}, \gamma = \frac{\mu \beta \sqrt{2\pi c}}{P_y}, \tau = \frac{\tau}{\rho u^2}$$

4.2.4 Solution of the problem

Expression for velocity, temperature and concentration profiles are obtained for equations (4.2.9) to (4.2.11) with initial and boundary condition (4.2.12) using the Laplace transform technique.

4.2.4.1 Solution of the problem for ramped temperature and ramped surface concentration

$$\theta(y, t) = f_6(y, t) - f_6(y, t - 1)H(t - 1) \quad (4.2.13)$$

$$C(y, t) = f_9(y, t) - f_9(y, t - 1)H(t - 1) \quad (4.2.14)$$

$$u(y, t) = g_1(y, t) + h_1(y, t) - h_1(y, t - 1)H(t - 1) \quad (4.2.15)$$

4.2.4.2 Solution of the problem for isothermal temperature and ramped surface concentration

In this case, the initial and boundary conditions are the same excluding Eq. (4.2.12) that becomes $\theta = 1$ at $y = 0, t \geq 0$.

$$\theta(y, t) = f_5(y, t) \quad (4.2.16)$$

$$C(y, t) = f_9(y, t) - f_9(y, t - 1)H(t - 1) \quad (4.2.17)$$

$$u(y, t) = h_2(y, t) + h_3(y, t) - h_3(y, t - 1)H(t - 1) \quad (4.2.18)$$

Where

$$h_1(y, t) = g_2(y, t) - g_3(y, t) - g_4(y, t) \quad (4.2.19)$$

$$h_2(y, t) = g_1(y, t) + g_5(y, t) - g_7(y, t) \quad (4.2.20)$$

$$h_3(y, t) = g_6(y, t) - g_4(y, t) \quad (4.2.21)$$

$$g_1(y, t) = \frac{e^{a't}}{2} \left[e^{-y\sqrt{\frac{1}{a}(b+a')}} \operatorname{erfc} \left(\frac{y}{2\sqrt{a't}} - \sqrt{(b+a')t} \right) + e^{y\sqrt{\frac{1}{a}(b+a')}} \operatorname{erfc} \left(\frac{y}{2\sqrt{a't}} + \sqrt{(b+a')t} \right) \right] \quad (4.2.22)$$

$$g_2(y, t) = a_{14}f_1(y, t) + a_{15}f_2(y, t) + a_9f_3(y, t) + a_{12}f_4(y, t) \quad (4.2.23)$$

$$g_3(y, t) = a_{10}f_5(y, t) + a_8f_6(y, t) + a_9f_7(y, t) \quad (4.2.24)$$

$$g_4(y, t) = a_{13}f_8(y, t) + a_{11}f_9(y, t) + a_{12}f_{10}(y, t) \quad (4.2.25)$$

$$g_5(y, t) = a_8f_1(y, t) - a_8f_3(y, t) \quad (4.2.26)$$

$$g_6(y, t) = a_{13}f_1(y, t) + a_{11}f_2(y, t) + a_{12}f_4(y, t) \quad (4.2.27)$$

$$g_7(y, s) = a_8 f_5(y, t) - a_8 f_7(y, t) \quad (4.2.28)$$

$$f_1(y, t) = \frac{1}{2} \left[e^{-y\sqrt{\frac{b}{a}}} \operatorname{erfc} \left(\frac{y}{2\sqrt{at}} - \sqrt{bt} \right) + e^{y\sqrt{\frac{b}{a}}} \operatorname{erfc} \left(\frac{y}{2\sqrt{at}} + \sqrt{bt} \right) \right] \quad (4.2.29)$$

$$f_2(y, t) = \frac{1}{2} \left[\left(t - \frac{y}{2\sqrt{ab}} \right) e^{-y\sqrt{\frac{b}{a}}} \operatorname{erfc} \left(\frac{y}{2\sqrt{at}} - \sqrt{bt} \right) + \left(t + \frac{y}{2\sqrt{ab}} \right) e^{y\sqrt{\frac{b}{a}}} \operatorname{erfc} \left(\frac{y}{2\sqrt{at}} + \sqrt{bt} \right) \right] \quad (4.2.30)$$

$$f_3(y, t) = \frac{e^{a_2 t}}{2} \left[e^{-y\sqrt{\frac{1}{a}(b+a_2)}} \operatorname{erfc} \left(\frac{y}{2\sqrt{at}} - \sqrt{(b+a_2)t} \right) + e^{y\sqrt{\frac{1}{a}(b+a_2)}} \operatorname{erfc} \left(\frac{y}{2\sqrt{at}} + \sqrt{(b+a_2)t} \right) \right] \quad (4.2.31)$$

$$f_4(y, t) = \frac{e^{-a_6 t}}{2} \left[e^{-y\sqrt{\frac{1}{a}(b-a_6)}} \operatorname{erfc} \left(\frac{y}{2\sqrt{at}} - \sqrt{(b-a_6)t} \right) + e^{y\sqrt{\frac{1}{a}(b-a_6)}} \operatorname{erfc} \left(\frac{y}{2\sqrt{at}} + \sqrt{(b-a_6)t} \right) \right] \quad (4.2.32)$$

$$f_5(y, t) = \operatorname{erfc} \left(\frac{y}{2\sqrt{dt}} \right) \quad (4.2.33)$$

$$f_6(y, t) = \left(\frac{y^2}{2d} + t \right) \operatorname{erfc} \left(\frac{y}{2\sqrt{dt}} \right) - \frac{y\sqrt{t}}{2\sqrt{d\pi}} e^{-\frac{y^2}{4dt}} \quad (4.2.34)$$

$$f_7(y, t) = \frac{e^{a_2 t}}{2} \left[e^{-y\sqrt{a_2/d}} \operatorname{erfc} \left(\frac{y}{2\sqrt{dt}} - \sqrt{a_2 t} \right) + e^{y\sqrt{a_2/d}} \operatorname{erfc} \left(\frac{y}{2\sqrt{dt}} + \sqrt{a_2 t} \right) \right] \quad (4.2.35)$$

$$f_8(y, t) = \frac{1}{2} \left[e^{-y\sqrt{KrSc}} \operatorname{erfc} \left(\frac{y\sqrt{Sc}}{2\sqrt{t}} - \sqrt{Krt} \right) + e^{y\sqrt{KrSc}} \operatorname{erfc} \left(\frac{y\sqrt{Sc}}{2\sqrt{t}} + \sqrt{Krt} \right) \right] \quad (4.2.36)$$

$$f_9(y, t) = \frac{1}{2} \left[\left(t - \frac{y\sqrt{Sc}}{2\sqrt{Kr}} \right) e^{-y\sqrt{ScKr}} \operatorname{erfc} \left(\frac{y\sqrt{Sc}}{2\sqrt{t}} - \sqrt{Krt} \right) + \left(t + \frac{y\sqrt{Sc}}{2\sqrt{Kr}} \right) e^{y\sqrt{ScKr}} \operatorname{erfc} \left(\frac{y\sqrt{Sc}}{2\sqrt{t}} + \sqrt{Krt} \right) \right] \quad (4.2.37)$$

$$f_{10}(y, t) = \frac{e^{-a_6 t}}{2} \left[e^{-y\sqrt{Sc(Kr-a_6)}} \operatorname{erfc} \left(\frac{y\sqrt{Sc}}{2\sqrt{t}} - \sqrt{(Kr-a_6)t} \right) + e^{y\sqrt{Sc(Kr-a_6)}} \operatorname{erfc} \left(\frac{y\sqrt{Sc}}{2\sqrt{t}} + \sqrt{(Kr-a_6)t} \right) \right] \quad (4.2.38)$$

4.2.4.3 Nusselt number, Sherwood number and Skin friction

Expressions of Nusselt number Nu for Ramped temperature and isothermal temperature are calculated from equations (4.2.13) and (4.2.16) using the relation

$$Nu = -\left(\frac{\partial\theta}{\partial y}\right)_{y=0} \quad (4.2.39)$$

For ramped wall temperature and ramped surface concentration:

$$Nu = -[I_6(t) - I_6(t - 1)H(t - 1)] \quad (4.2.40)$$

For isothermal temperature and ramped surface concentration:

$$Nu = -[I_5(t)] \quad (4.2.41)$$

Expressions of Sherwood number Sh for Ramped temperature and isothermal temperature are calculated from equations (4.2.14) and (4.2.17) using the relation

$$sh = -\left(\frac{\partial C}{\partial y}\right)_{y=0} \quad (4.2.42)$$

For ramped wall temperature and ramped surface concentration:

$$Sh = -[I_9(t) - I_9(t - 1)H(t - 1)] \quad (4.2.43)$$

For isothermal temperature and ramped surface concentration:

$$Sh = -[I_9(t) - I_9(t - 1)H(t - 1)] \quad (4.2.44)$$

Expressions of skin-friction for Ramped temperature and isothermal temperature are calculated from Equations (4.2.15) and (4.2.18) using the relations

$$\tau^*(y, t) = -\mu\beta\left(1 + \frac{1}{\gamma}\right)\tau \quad (4.2.45)$$

Where $\tau = \left.\frac{\partial u}{\partial y}\right|_{y=0}$ (4.2.46)

For ramped wall temperature and ramped surface concentration:

$$\tau = I_{11}(t) + I_{18}(t) - I_{18}(t - 1)H(t - 1) \quad (4.2.47)$$

For isothermal temperature and ramped surface concentration:

$$\tau = I_{19}(t) + I_{20}(t) - I_{20}(t-1)H(t-1) \quad (4.2.48)$$

Where

$$I_1(t) = -\sqrt{\frac{b}{a}} \operatorname{erf}(\sqrt{bt}) - \frac{e^{-bt}}{\sqrt{\pi at}} \quad (4.2.49)$$

$$I_2(t) = -\frac{1}{\sqrt{4ab}} \operatorname{erf}(\sqrt{bt}) - t \sqrt{\frac{b}{a}} \operatorname{erf}(\sqrt{bt}) - \frac{t e^{-bt}}{\sqrt{\pi at}} \quad (4.2.50)$$

$$I_3(t) = -e^{a_2 t} \sqrt{\frac{b+a_2}{a}} \operatorname{erf}(\sqrt{(b+a_2)t}) - \frac{e^{-bt}}{\sqrt{\pi at}} \quad (4.2.51)$$

$$I_4(t) = -e^{-a_6 t} \sqrt{\frac{b-a_6}{a}} \operatorname{erf}(\sqrt{(b-a_6)t}) - \frac{e^{-bt}}{\sqrt{\pi at}} \quad (4.2.52)$$

$$I_5(t) = -\sqrt{\frac{1}{\pi t d}} \quad (4.2.53)$$

$$I_6(t) = -2 \sqrt{\frac{t}{d \pi}} \quad (4.2.54)$$

$$I_7(t) = -e^{a_2 t} \sqrt{a_2/d} \operatorname{erf}(\sqrt{a_2 t}) - \sqrt{\frac{1}{d \pi t}} \quad (4.2.55)$$

$$I_8(t) = -\sqrt{Kr Sc} \operatorname{erf}(\sqrt{Kr t}) - \sqrt{\frac{Sc}{\pi t}} e^{-Kr t} \quad (4.2.56)$$

$$I_9(t) = -\sqrt{\frac{Sc}{4 Kr}} \operatorname{erf}(\sqrt{Kr t}) - t \sqrt{Sc Kr} \operatorname{erf}(\sqrt{Kr t}) - \sqrt{\frac{t Sc}{\pi}} e^{-Kr t} \quad (4.2.57)$$

$$I_{10}(t) = -e^{-a_6 t} \sqrt{Sc(Kr - a_6)} \operatorname{erf}(\sqrt{(Kr - a_6)t}) - \sqrt{\frac{Sc}{\pi t}} e^{-Kr t} \quad (4.2.58)$$

$$I_{11}(t) = -e^{a' t} \sqrt{\frac{b+a'}{a}} \operatorname{erf}(\sqrt{(b+a')t}) - \frac{e^{-bt}}{\sqrt{\pi at}} \quad (4.2.59)$$

$$I_{12}(t) = a_{14} I_1(t) + a_{15} I_2(t) + a_9 I_3(t) + a_{12} I_4(t) \quad (4.2.60)$$

$$I_{13}(t) = a_{10} I_5(t) + a_8 I_6(t) + a_9 I_7(t) \quad (4.2.61)$$

$$I_{14}(t) = a_{13} I_8(t) + a_{11} I_9(t) + a_{12} I_{10}(t) \quad (4.2.62)$$

$$I_{15}(t) = a_8 I_1(t) - a_8 I_3(t) \quad (4.2.63)$$

$$I_{16}(t) = a_{13} I_1(t) + a_{11} I_2(t) + a_{12} I_4(t) \quad (4.2.64)$$

$$I_{17}(t) = a_8 I_5(t) - a_8 I_7(t) \quad (4.2.65)$$

$$I_{18}(t) = I_{12}(t) - I_{13}(t) - I_{14}(t) \quad (4.2.66)$$

$$I_{19}(t) = I_{11}(t) + I_{15}(t) - I_{17}(t) \quad (4.2.67)$$

$$I_{20}(t) = I_{16}(t) - I_{14}(t) \quad (4.2.68)$$

4.2.5 Results and discussion

Fluid velocity, temperature and concentration profiles for several values of Casson parameter γ , magnetic parameter M , radiation parameter Nr , chemical reaction parameter Kr and permeability of porous medium k are presented in Figure 4.2.2 to Figure 4.2.10.

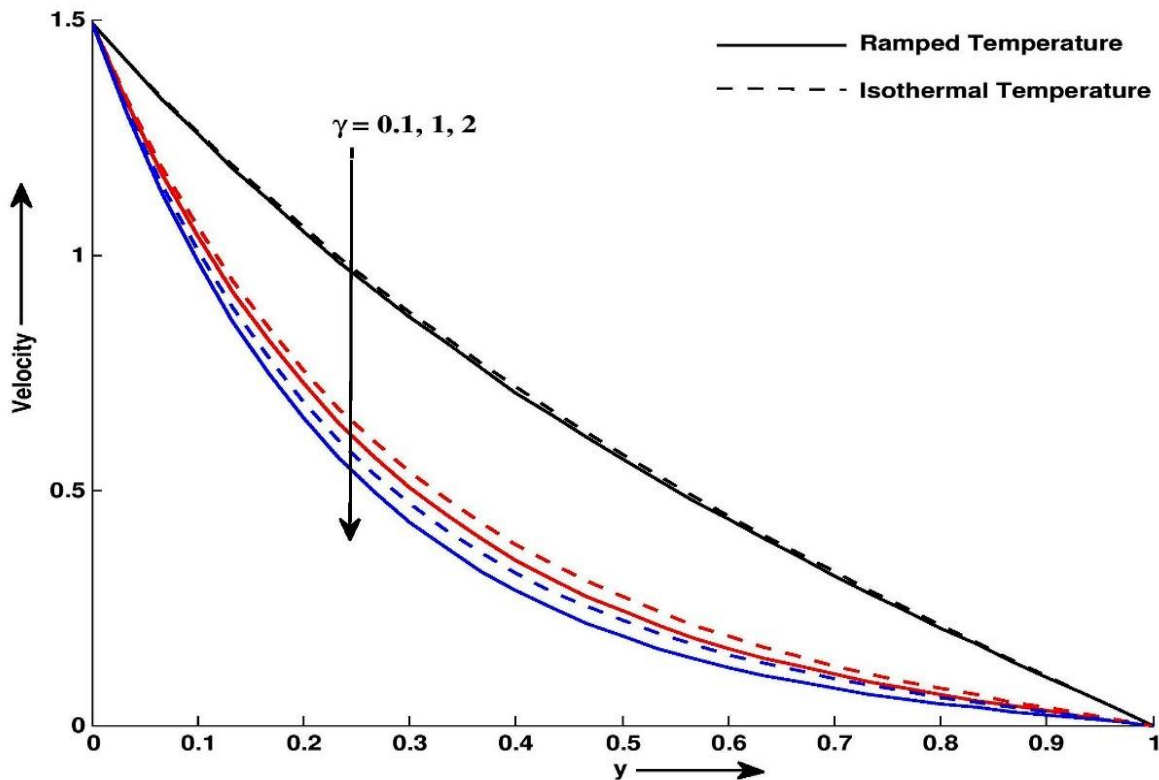


Figure 4.2.2: Velocity profile u for different values of y and γ at $M = 5, k = 0.5, Pr = 15, Sc = 0.66, Gm = 3, Gr = 4, Nr = 5, Kr = 5$ and $t = 0.4$

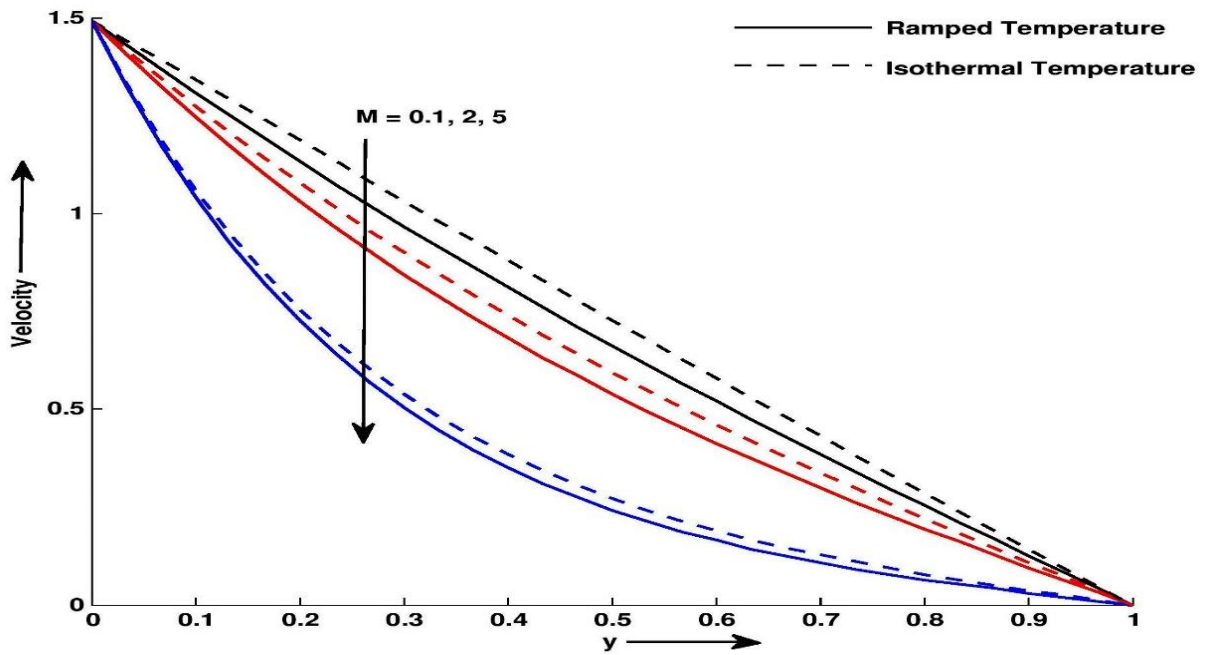


Figure 4.2.3: Velocity profile u for different values of y and M at $\gamma = 1, k = 0.5, Pr = 15, Sc = 0.66, Gm = 3, Gr = 4, Nr = 5, Kr = 5$ and $t = 0.4$

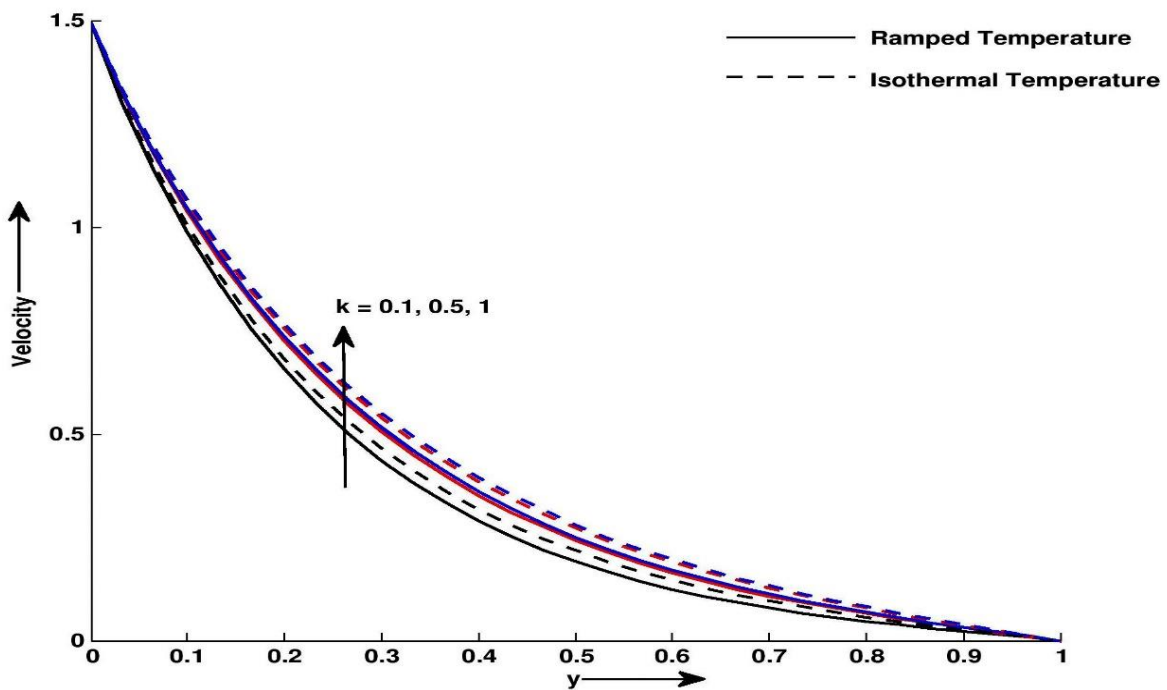


Figure 4.2.4: Velocity profile u for different values of y and k at $\gamma = 1, M = 5, Pr = 15, Sc = 0.66, Gm = 3, Gr = 4, Nr = 5, Kr = 5$ and $t = 0.4$

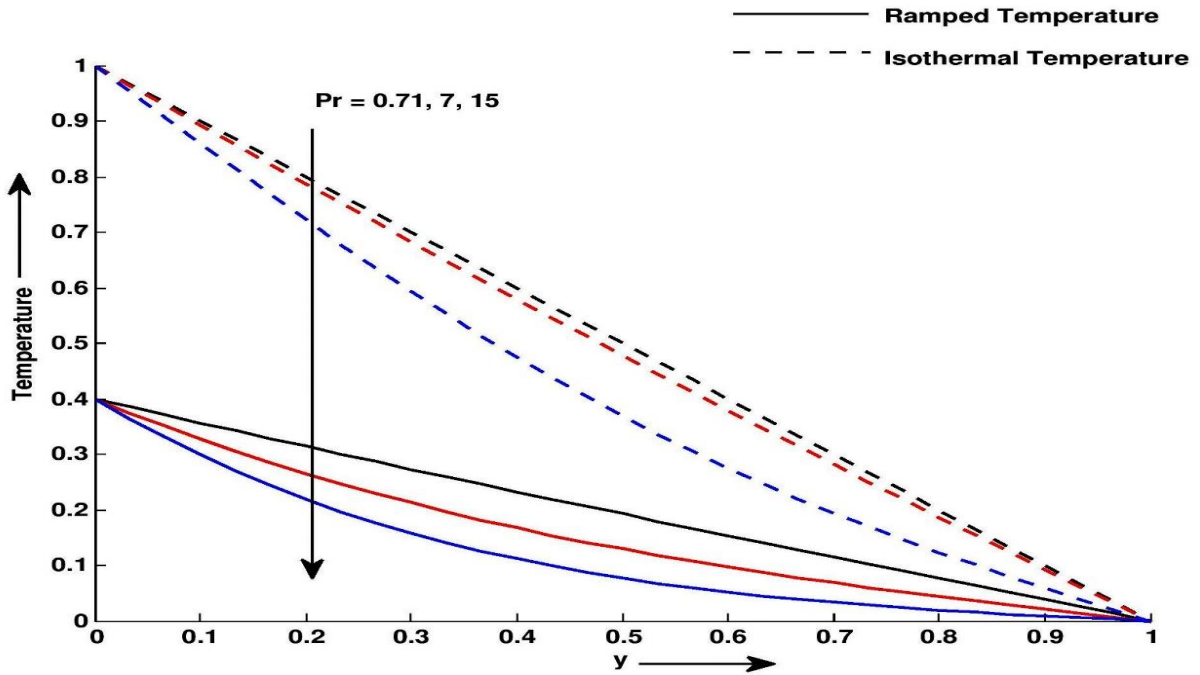


Figure 4.2.5: Temperature profile θ for different values of y and Pr at $Nr = 5$ and $t = 0.4$

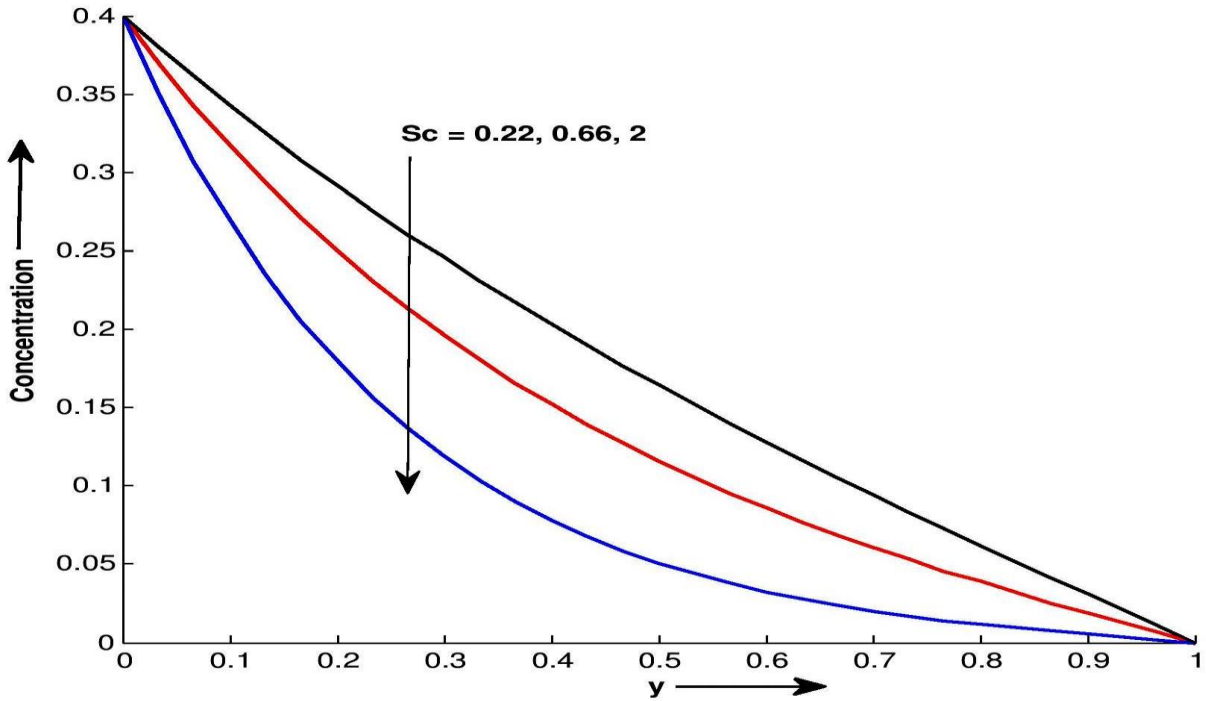


Figure 4.2.6: Concentration profile C for different values of y and Sc at $Kr = 5$ and $t = 0.4$.

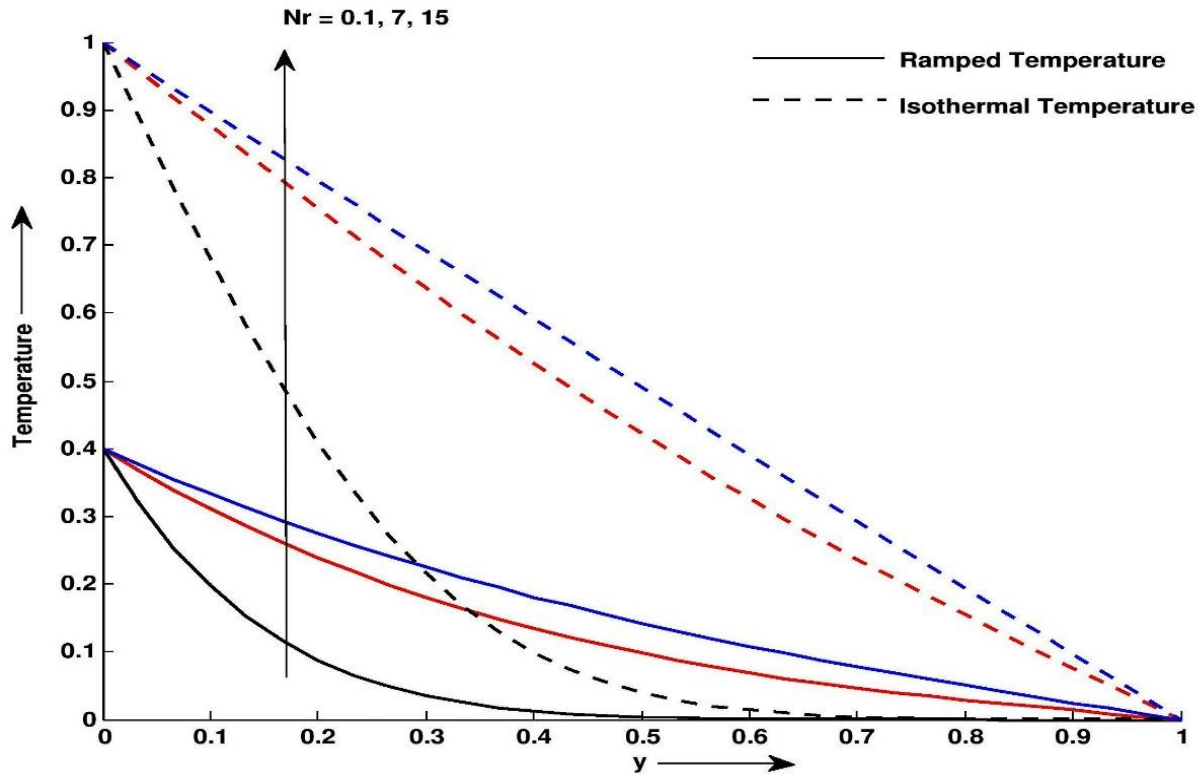


Figure 4.2.7: Temperature profile θ for different values of y and Kr at $Pr = 15$ and $t = 0.4$

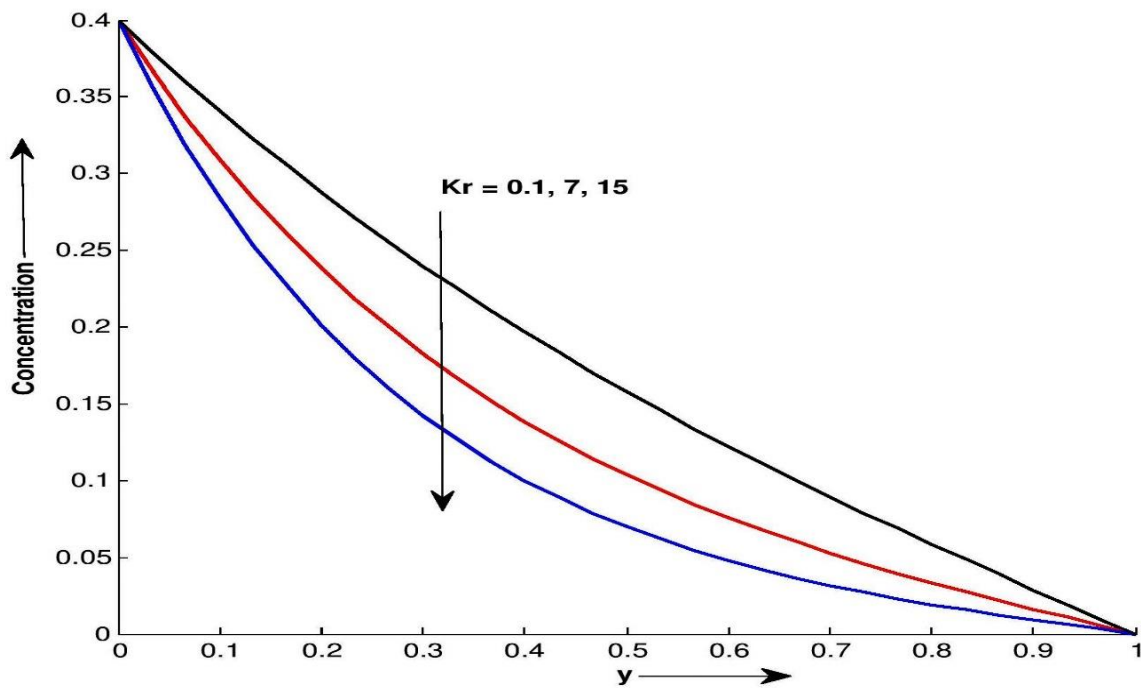


Figure 4.2.8: Concentration profile C for different values of y and Kr at $Sc = 0.66$ and $t = 0.4$

Figure 4.2.2 shows effect of Casson fluid parameter γ on velocity profile for both thermal conditions. It is seen that velocity profile decreases with increase in Casson fluid parameter γ . It occurs because of plasticity of Casson fluid. The plasticity of the fluid increases with decrease in Casson parameter. It causes the increment in velocity boundary layer thickness. Figure 4.2.3 displays the effect of magnetic parameter M on the velocity profiles. It is seen that the amplitude of the motion as well as the boundary layer thickness decreases when M is increased. Figure 4.2.4 illustrates that effect of permeability of porous medium k on velocity profile. It is observed that for increasing values of k , the resistance of the porous medium is lowered which increases the momentum development of the flow regime. Figure 4.2.5 shows effect of Prandtl number Pr on temperature profile. For both thermal conditions, it is seen that Prandtl number Pr tends to reduce heat transfer process. In heat transfer problems, the Prandtl number controls thickness of the momentum and thermal boundary layers. This means that for liquid metals, thickness of the temperature boundary layer is much bigger than the momentum boundary layer. Effect of Schmidt number Sc on concentration profiles is shown in Figure 4.2.6. It is seen that, the concentration near the plate gets reducing the thickness this leads minimizing the mass buoyancy force due to enhancement in the values of Sc . Figure 4.2.7 shows that effect of thermal radiation Parameter Nr on Temperature profile. It is observed that temperature is increase with increase in Nr . It is noticed that thermal radiation parameter reduces thermal buoyancy force, minimizing the thickness of the thermal boundary layer. Therefor temperature profiles increase with increase in radiation parameter Nr . Chemical reaction has a delaying effect on concentration profile for both thermal cases as shown in Figure 4.2.8. This shows that the $Kr > 0$ leads to fall in the concentration field which in turn declines the buoyancy effects due to concentration gradients. Consequently, the flow field is retarded. This occurrence has a superior agreement with the physical realities.

Table 4.2.1: Skin friction variation

Pr	γ	Sc	Gr	Gm	Kr	M	k	Nr	t	Skin friction τ for Ramped temperature	Skin friction τ for isothermal temperature
10	0.9	0.66	2	3	2	1	0.8	3	0.3	6.8445	6.4381
11	0.9	0.66	2	3	2	1	0.8	3	0.3	6.8478	6.4539
12	0.9	0.66	2	3	2	1	0.8	3	0.3	6.8508	6.4681

10	1.0	0.66	2	3	2	1	0.8	3	0.3	9.6725	9.2700
10	1.1	0.66	2	3	2	1	0.8	3	0.3	16.3901	15.9910
10	0.9	0.7	2	3	2	1	0.8	3	0.3	5.4086	5.0022
10	0.9	1.0	2	3	2	1	0.8	3	0.3	3.7118	3.3054
10	0.9	0.66	2.1	3	2	1	0.8	3	0.3	6.8393	6.4126
10	0.9	0.66	2.2	3	2	1	0.8	3	0.3	6.8340	6.3870
10	0.9	0.66	2	3.1	2	1	0.8	3	0.3	6.9520	6.5457
10	0.9	0.66	2	3.2	2	1	0.8	3	0.3	7.0596	6.6532
10	0.9	0.66	2	3	2.1	1	0.8	3	0.3	4.5998	4.1935
10	0.9	0.66	2	3	2.2	1	0.8	3	0.3	3.6534	3.2471
10	0.9	0.66	2	3	2	1.1	0.8	3	0.3	22.6077	22.2038
10	0.9	0.66	2	3	2	1.2	0.8	3	0.3	374.0227	373.6214
10	0.9	0.66	2	3	2	1	0.9	3	0.3	4.2335	3.8255
10	0.9	0.66	2	3	2	1	1.0	3	0.3	3.2818	2.8725
10	0.9	0.66	2	3	2	1	0.8	3.1	0.3	6.8436	6.4340
10	0.9	0.66	2	3	2	1	0.8	3.2	0.3	6.8428	6.4300
10	0.9	0.66	2	3	2	1	0.8	3	0.4	6.9344	6.5148
10	0.9	0.66	2	3	2	1	0.8	3	0.5	6.9807	6.5655

Table 4.2.2: Nusselt number variation

Pr	Nr	t	Nusselt number Nu for Ramped Temperature	Nusselt number Nu for isothermal Temperature
10	3	0.3	0.9772	1.6287
11	3	0.3	1.0249	1.7082
12	3	0.3	1.0705	1.7841
10	3.1	0.3	0.9652	1.6087
10	3.2	0.3	0.9537	1.5894
10	3	0.4	1.1284	1.4105
10	3	0.5	1.2616	1.2616

Table 4.2.3: Sherwood number variation

Sc	t	Sherwood number for Ramped wall concentration Sh
0.66	0.3	0.5970
0.7	0.3	0.6148
1.0	0.3	0.7348
0.66	0.3	0.6014
0.66	0.3	0.6059
0.66	0.4	0.7233
0.66	0.5	0.8454

Table 4.2.4: Comparison of Sherwood number with Ref. [150]

t	Kr	Sc	Sherwood number Sh for ramped temp. Ref [150]	Sherwood number Nu for ramped temp.	Sherwood number Sh for isothermal temp. Ref [150]	Sherwood number Sh for isothermal temp.
0.3	0.2	0.22	0.295649	0.2956	0.525702	0.5257
0.5	0.2	0.22	0.386593	0.3866	0.428415	0.4284
0.7	0.2	0.22	0.463189	0.4632	0.379505	0.3796
0.3	2.0	0.22	0.344659	0.3447	0.839945	0.8399
0.5	2.0	0.22	0.488076	0.4881	0.785973	0.7860
0.7	2.0	0.22	0.625355	0.6254	0.757863	0.7579
0.3	5.0	0.22	0.416933	0.4169	1.1897	1.1897
0.5	5.0	0.22	0.628694	0.6287	1.12945	1.1294
0.7	5.0	0.22	0.838894	0.8389	1.09522	1.0952

Table 4.2.5: Comparison of Nusselt number with Ref. [141]

t	Nr	Pr	Nusselt number Nu for ramped temp. Ref [141]	Nusselt number Nu for ramped temp.	Nusselt number Nu for isothermal temp. Ref [141]	Nusselt number Nu for isothermal temp.
0.2	0.5	0.71	0.3472	0.3472	0.8679	0.8679
0.4	0.5	0.71	0.4910	0.4910	0.6137	0.6137

Chapter 4:

0.6	0.5	0.71	0.6013	0.6013	0.5011	0.5011
0.8	0.5	0.71	0.6944	0.6944	0.4340	0.4340
1.0	0.5	0.71	0.7763	0.7763	0.3882	0.3882
1.2	0.5	0.71	0.5032	0.5032	0.3543	0.3543
1.4	0.5	0.71	0.4276	0.4276	0.3281	0.3281
0.2	1.0	0.71	0.3007	0.3007	0.7517	0.7517
0.4	1.0	0.71	0.4252	0.4252	0.5315	0.5315
0.6	1.0	0.71	0.5208	0.5208	0.4340	0.4340
0.8	1.0	0.71	0.6013	0.6013	0.3758	0.3758
1.0	1.0	0.71	0.6723	0.6723	0.3362	0.3362
1.2	1.0	0.71	0.4358	0.4358	0.3069	0.3069
1.4	1.0	0.71	0.3703	0.3703	0.2841	0.2841
0.2	5.0	0.71	0.1736	0.1736	0.4340	0.4340
0.4	5.0	0.71	0.2455	0.2455	0.3069	0.3069
0.6	5.0	0.71	0.3007	0.3007	0.2506	0.2506
0.8	5.0	0.71	0.3472	0.3472	0.2170	0.2170
1.0	5.0	0.71	0.3882	0.3882	0.1941	0.1941
1.2	5.0	0.71	0.2516	0.2516	0.1772	0.1772
1.4	5.0	0.71	0.2138	0.2138	0.1640	0.1640
0.2	10	0.71	0.1282	0.1282	0.3205	0.3205
0.4	10	0.71	0.1813	0.1813	0.2266	0.2266
0.6	10	0.71	0.2221	0.2221	0.1850	0.1850

0.8	10	0.71	0.2564	0.2564	0.1603	0.1603
1.0	10	0.71	0.2867	0.2867	0.1433	0.1433
1.2	10	0.71	0.1858	0.1858	0.1308	0.1308
1.4	10	0.71	0.1579	0.1579	0.1211	0.1211

Table 4.2.1 shows effects of governing parameter on Skin friction for both thermal conditions. It is observed that, Schmidt number Sc , thermal Grashof number Gr , chemical reaction Kr , permeability of porous medium k and thermal radiation parameter Nr tends to reduce Skin friction whereas, Prandtl number Pr , Casson fluid γ , mass Grashof number Gm , Magnetic field M and time t has reverse effect on it. Table 4.2.2 shows influence of Prandtl number Pr , thermal radiation parameter Nr and time t on Nusselt number. For both thermal conditions, it is seen that Nr tends to reduce rate of heat transfer whereas, Pr has reverse effect on it. Table 4.2.3 shows concentration gradient at the surface increase with increase in Kr, Sc and t . Table 4.2.4 validates our results in terms of Sherwood number as it shows strong agreement with Seth et al. [150], whereas Table 4.2.5 strengthens values of Nusselt number by comparing with those of Seth et al. [141].

4.2.6 Conclusion

Concluding remarks can be summarized as follows:

- Casson fluid parameter γ and Magnetic field M tend to reduce momentum whereas permeability of porous medium k has reverse effect on it throughout the flow field.
- Heat transfer process improve with thermal radiation parameter Nr .
- Concentration decrease tendency with chemical reaction Kr and Schmidt Number Sc .
- For both thermal plates, Skin friction and Nusselt number increases with increase in Pr, γ, Gm, M and t while decrease with increase in Nr, Sc, Gr, Kr and k .
- Rate of mass transfer get reduced with Sc, Kr and t .
- Rate of Heat transfer get reduced with Nr , whereas improves with Pr .